AIAA JOURNAL
Vol. 45, No. 3, March 2007

Active Store Trajectory Control in Supersonic Cavities Using Microjets and Low-Order Modeling

Debashis Sahoo and Anuradha Annaswamy
Massachusetts Institute of Technology, Cambridge, Massachusetts 02139
and
Farrukh Alvi
Florida A&M University and Florida State University, Tallahassee, Florida 32310

DOI: 10.2514/1.18007

Recently, there has been a concerted effort in controlling the trajectory of a store departing from a cavity in a supersonic flow so as to ensure safe separation. The candidate actuator that has achieved a safe departure in model-scale wind tunnel tests using minimum flow rate is a tandem array of microjets placed in the spanwise direction near the leading edge of the cavity. In this paper, a low-order model is derived that captures the dominant mechanisms that govern the store trajectory with and without microjets and conditions under which unsafe and safe departures occur are predicted. This model includes separate components to predict the pitch and plunge motion of the store when it is inside the cavity, when it is passing through the shear layer at the mouth of the cavity and when it is completely outside the cavity. The model derivations are based on the assumptions of store ejection from the cavity middle, slender axisymmetric body aerodynamics, thin shear layer at the cavity mouth, high Reynolds number external crossflow, plane shock waves associated with the microjet actuators, and quiescent cavity. The model predictions are compared to the results of store drop experiments performed under the HIFEX Program at Mach 2.0 and 2.46 using a generic subscale weapons bay for different control inputs. It was found that the model predictions qualitatively corroborate the main experimental observations that 1) the store drop is unsuccessful for the microjet-off case, 2) the store departs safely under small microjet pressures, and 3) the store returns back to the cavity under large microjet pressures, under certain operating conditions. The model is extended to include the effect of the shear layer thickness and its predictions compared more favorably to the experimental results than the original model in certain conditions. Finally, the optimal control input to ensure clean store departure for a host of drop conditions is predicted using the low-order model.

Nomenclature

A	=	$\hat{\rho}_\infty \delta \hat{l}_o^3 g_4/\hat{m}_s$
$(A)_\mu$	=	dimensional microjet cross-section area
$a(x)$	=	store radius at x
B	=	$\hat{l}_o g_6/\lvert h_6\rvert$
C_μ	=	microjet-crossflow momentum ratio
D_o	=	cavity width
F, M	=	store normal force and pitching moment (from store-induced potential)
F_w, M_w	=	store normal force and pitching moment (from shear layer profile)
G_0, G_1, G_2	=	zero, first-, and second-order store cross-section area moments
g	=	acceleration due to gravity
$g_0, \ldots, g_{11}, h_0, \ldots, h_{11}$	=	factors in the expression for F and M
H_o	=	cavity depth
$h(X') = W_i \cos(\lambda_i X' + \zeta_i) + R_i$	=	wavy profile , as defined in Eq. (3)
L_o	=	cavity length
l_o	=	store length
M	=	external flow Mach number
$(\hat{m}_s, \hat{I}_s)$	=	store mass and moment of inertia about its axis
$(N)_\mu$	=	number of microjets
$O(q)$	=	$0 < \lvert\cdot\rvert < q$
t	=	time
t_o	=	characteristic time scale for store plunge
U	=	mean dimensional crossflow speed
(X, Y, Z)	=	cavity-attached coordinate system for store-induced potential
(X', Y', Z')	=	cavity-attached coordinate system for shear layer profile related dynamics
X'_c	=	store c.g. streamwise coordinate
x	=	axial distance of a store point from its c.g.
(x_o, x_e)	=	axial distance of store nose, tail from its c.g.
(Y, α, V, ω)	=	store vertical coordinate, angle of attack, plunge, and pitch rates measured at its c.g.
α	=	$\frac{\hat{\alpha}}{\delta}$
$\hat{\alpha}$	=	store angle of attack
β	=	$\sqrt{M_{\infty,r}^2 - 1}$
γ	=	ratio of specific heats
δ	=	ratio of maximum store radius to length

Presented as Paper 3097 at the AIAA/CEAS Aeroacoustics Conference, Monterey, CA, 23–26 May 2005; received 18 June 2005; revision received 19 September 2006; accepted for publication 30 October 2006.

δ_s = shear layer profile thickness
θ = flow bending angle after passing through shock
ρ = external freestream density
ψ = shock orientation angle

Subscripts

c = measured at any time at the store c.g.
r = freestream condition relative to shear layer profile
0 = measured at the time of store release inside cavity
1 = measured at the time of store exit from cavity
μ = measured at microjet nozzle exit
∞ = freestream condition

Superscript

$\hat{}$ = indicates dimensional values; its absence typically indicates nondimensional values, unless otherwise mentioned

I. Introduction

IT HAS been observed that a store, when released from an internal aircraft bay, can return back under subsonic [1], transonic [2], and supersonic [3–5] flight conditions. To ameliorate the problem of unsafe store separation, the recently commenced Defense Advanced Research Projects Agency (DARPA)-funded HIFEX Program [3–5] has used an active control method to ensure safe release of a slender axisymmetric store from a rectangular cavity (bay) with an external supersonic flow. The effectiveness of various flow control actuators has been studied under this program. The most promising one that guarantees safe store separation over a range of operating conditions while using a minimum amount of mass flow rate was observed to be a tandem array of microjet flow injectors distributed in the spanwise direction near the leading edge of the cavity. By varying the pressure at which the microjets are activated, it was observed that successful store separation was achievable even as the operating conditions changed [3].

Despite these studies, the underlying mechanism that governs the store separation from a cavity in supersonic flow is currently unknown. Also unknown are the limiting conditions under which the store can be dropped from the cavity to achieve safe separation. Finally, the dominant mechanism underlying the impact of microjets on the store release trajectory is also not understood. The need therefore arises for a model that addresses these issues and that accurately predicts the trend in the store trajectory, that is, whether the store is ejected from the cavity safely or returns back into the cavity, under given initial drop conditions and a given control input. The model should also be reduced order and parametric in order to be applied for developing the optimal control strategy that guarantees safe store separation over a range of operating conditions.

From a preliminary investigation of the dominant physics of the problem, it can be said that the trend in the store trajectory is possibly influenced by a host of factors (Fig. 1), including the inhomogeneous flowfield generated by the wavy shear layer profile at the cavity opening, the potential induced by the store motion, and the shock waves introduced by the microjets, all of which should be incorporated in the model. What is examined in this paper, in particular, is an investigation of the forces and moments on the store due to these factors, a low-order model based on these store loads, and an optimal control design for safe store separation. The following effects have not been explicitly modeled in this paper: the cavity acoustics field, the mean inner cavity flowfield, and the shock waves

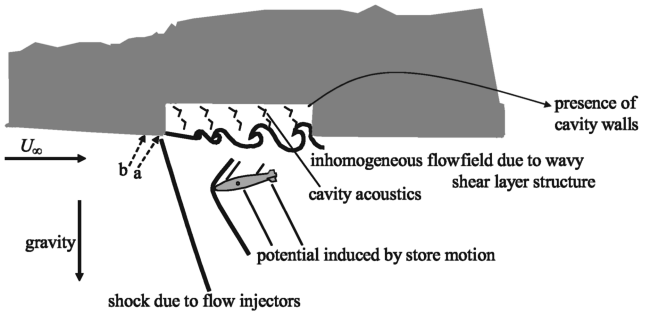

Fig. 1 Different factors affecting the store release trajectory under supersonic crossflow and in the presence of microjet-based actuators. Labels "a" and "b" indicate different rows of microjets located near the cavity leading edge.

associated with the store as it traverses the shear layer and drops outside the cavity, as explained subsequently. It may be noted that the shear layer profile and the cavity acoustic field are elements of a feedback loop; hence, by including the shear layer profile, the cavity acoustics are indirectly accounted for in the model.

A. Background

The dynamics of a slender body separating from a rectangular cavity under a crossflow is difficult to analyze, expensive to experiment upon, and is mostly used for military applications. As such, limited models are available in literature and the pertinent ones are outlined here. The problem of store release from a cavity under subsonic flow has been extensively analyzed by Shalaev et al. [1]. In the said reference, a low-order model of the store dynamics is derived, based on slender body potential flow theory, and results in a set of ordinary differential equations for the store motion which is analytically solvable under suitable conditions. It was possible to develop the simplified model because of the subsonic flow conditions and simplifications associated with the store geometry. This model is shown to predict the store trajectories observed in subsonic wind tunnel experiments. In [2], the store separation from a cavity under transonic flow has been studied by the same authors. The model in [2] is similar to that in [1], but includes nonlinear differential equations for the store dynamics. These equations cannot be solved analytically because of the transonic flow conditions. However, physically reasonable simplifications were applied to the model to derive conditions under which unsafe store departure occurs in transonic flow regime. Finally in Malmuth and Shalaev [6], the problem of store separation from a parent body in supersonic flow is considered, with the treatment being similar to Shalaev et al. [2]. In particular, Malmuth and Shalaev [6] predict the store interaction with shock waves due to the parent body after the store has separated from the body. This paper takes two steps further, compared to Shalaev et al. [1,2,6]. First, this paper quantitatively identifies the dominant mechanisms that govern the store trajectory when dropped from a cavity into supersonic stream, by extending the techniques developed in these references. Second, the paper quantitatively identifies the dominant mechanisms introduced when the microjets are switched on at the cavity leading edge during the drop.

Because the approach used in this paper is based on Shalaev et al. [1,2,6], a summary of the low-order model of the store dynamics developed in these references is included. The model is restricted to the pitch and plunge motion of the store. The latter is assumed to be a slender, axisymmetric body with a small angle of attack and dropped near the cavity middle. The flowfield assumptions are quiescent inside the cavity, a thin shear layer compared to the cavity length, and a high Reynolds number external crossflow. These assumptions allow the use of a potential function in solving the velocity field associated with the store motion.

The velocity potential is then shown to satisfy the Laplace equation in the cross-section plane of the store. Owing to linearity, the Laplace equation is solved separately for the cases when the store was inside the cavity, when it crosses the shear layer, and when it is

completely outside the cavity. The technique used for solving the Laplace equation is a combination of multiple expansion and conformal transformation. The latter procedure is outlined in [1]. The resulting velocity field is converted to pressure through the unsteady Bernoulli's equation. The pressure is integrated along the store surface to obtain normal force and pitching moment on the store. By using Newton's second law, the store trajectory is computed. Using this method, Malmuth and Shalaev [6] predict the conditions for unsafe store ejection.

An alternative approach for external store separation found in the literature [7] is based on grid testing. In this method, the store aerodynamic load at any position in the grid is assumed to be a function of only its freestream aerodynamics and the parent aircraft induced aerodynamics with no mutual interference. A linear interference effect between the store and parent body is introduced in a store separation problem for the SH-2G helicopter [8]. This method is validated by comparing with experimentally available store release trajectory data. However, this approach is limited by lack of available freestream data for all possible store shapes and pitch angles, lack of physical insight into the problem, and expensive experiments required. The approach has not been further explored in this paper.

The goal of this paper is mainly to study the effect of microjets on the store trajectory. For this purpose, the low-order model developed in [1,2,6] is extended to incorporate the effects of microjets. This is done by determining the dominant mechanisms that 1) govern the store trajectory in the absence of microjets, and 2) are introduced due to the addition of microjets. By using a careful investigation of the force and moment expressions on the store obtained from the said references, we obtain a set of parametric nonlinear ordinary differential equations that enables us to identify the mechanism and, therefore, the criteria for unsafe store release from a cavity in general. The paper next identifies the microjet-crossflow momentum ratio as one of the most relevant control parameters for this problem and investigates the underlying process by which the store trajectory is influenced by the momentum ratio. These two steps of identification and subsequent investigation of the dominant control parameter are the most important contributions of the current paper. The model is also used to predict the optimal microjet pressure distribution for a safe weapon release and this control strategy is shown to agree with experimental observations made under the DARPA-funded HIFEX Program [3–5] for different supersonic Mach numbers. Finally, the model suggests better choices for the actuator parameters at some of the operating conditions.

II. Store Release Model Development

The model in this section is derived from the low-order ones developed in [1,2,6]. The starting problem considered is the first-order effect of the wavy shear layer profile on the normal force and pitching moment on the store. In the subsequent problem, the force and moment expressions are investigated in detail as the store drops from the cavity in the absence and presence of microjets. The two problems are finally compared with each other.

A. Contribution of Wavy Shear Layer Structures

First, we consider the effect of the wavy shear layer profile on the normal force and pitching moment on the store. The wavy profile is governed by shedding of vortices at the cavity mouth which in turn is excited by the cavity acoustic field, leading to a feedback loop between the two [9]. The wavy profile results in nonuniformity in the flow domain outside the cavity that potentially change the aerodynamic loads on the store. The expression for the resulting loads is adopted from Malmuth and Shalaev [6]. An order of magnitude analysis is then performed on the force and moment expressions to quantify the effect of the wavy profile.

We follow the nondimensional scheme given by

$$X' = \frac{\hat{X}}{\hat{L}_o}, \qquad Y' = \frac{\hat{Y}}{\hat{L}_o}, \qquad Z' = \frac{\hat{Z}}{\hat{L}_o} \tag{1}$$

Let the nondimensional wavy profile be given by

$$Y'_w = \delta_s h(X'), \qquad h(\cdot) = O(1) \tag{2}$$

Also, without any loss of generality, we assume that the wavy profile consists of piecewise cosine components, such as

$$h(X') = W_i \cos(\lambda_i X' + \zeta_i) + R_i \tag{3}$$

where i is an integer, and $W_i = O(1)$. It was observed from flow visualization studies (see Fig. 10) that λ_i is typically $O(10)$. Then we have the following expressions for the normal force F_w and pitching moment M_w on the store:

$$|F_w| \le \pi\mu\delta_s\delta \max_i(W_i\lambda_i^2)G_0 \qquad |M_w| \le \pi\mu\delta_s\delta \max_i(W_i\lambda_i^2)G_1 \tag{4}$$

where $G_0 = \int_{x_o}^{x_e} a^2(x)\,\mathrm{d}x$, $G_1 = \int_{x_o}^{x_e} a^2(x)x\,\mathrm{d}x$, $x = \hat{x}/\hat{l}_o$ (see Fig. E1 in Appendix E), $a = \hat{a}/\delta\hat{l}_o$, (x_o, x_e) are the nose and tail coordinates of the store, and $\mu = (\hat{l}_o/\hat{L}_o) \le O(1)$. Also, F_w and M_w are nondimensionalized by $(\hat{\rho}_\infty U_\infty^2)_r \delta \hat{l}_o^2$ and $(\hat{\rho}_\infty U_\infty^2)_r \delta \hat{l}_o^3$, respectively, where $(\hat{\rho}_\infty U_\infty^2)_r$ is the dynamic pressure of the external crossflow velocity relative to the wavy shear layer profile. It may be noted that $G_0 \le O(1)$, $G_1 \le O(1)$, $\delta \ll 1$, and $\delta_s \ll 1$. Moreover, another effect induced by the wavy shear layer profile is additional vertical velocity on the body surface (leading to increase in local angle of attack). The relevant expression is given in [6].

It is clear that the contribution of the wavy profile to F_w and M_w is proportional in magnitude to the thickness of the profile. The smaller the wavy profile in thickness, the smaller is their influence on F_w and M_w. The comparison between the contributions of the wavy shear layer thickness and the store motion induced potential to the store loads is given in Sec. II.F. The definition of a "thin" shear layer is also presented in the section.

B. Contribution of Store Motion Induced Velocity Potential

The first-order force and moment expressions due to the store falling down from the quiescent cavity with a thin shear layer are given in [2]. These expressions are further processed in the current paper to obtain a set of parametric nonlinear ordinary differential equations for the store trajectory. We develop the appropriate parametric expressions for the force and moment in three stages: 1) when the store is completely inside the cavity (problems 1a and 2a in the reference), 2) when the store passes through the shear layer (problem 3 in the reference), and 3) when the store is completely outside the cavity (problems 2b in the reference).

C. Force and Moment for Store Inside Cavity

When the store is completely inside the cavity, the resulting normal force and pitching moment on the store, expressed in a parametric form, are given by

$$\hat{F} = \pi\hat{\rho}_\infty\delta\hat{l}_o^3\left(g_0\frac{\mathrm{d}\hat{V}_c}{\mathrm{d}\hat{t}}\hat{l}_o + g_1\frac{\mathrm{d}\hat{\omega}}{\mathrm{d}\hat{t}}\hat{l}_o^2 + g_2\hat{\omega}^2\hat{l}_o^2 + g_4\hat{V}_c^2 + g_9\hat{\omega}\hat{l}_o\hat{V}_c\right)$$

$$\hat{M} = \pi\hat{\rho}_\infty\delta\hat{l}_o^4\left(h_0\frac{\mathrm{d}\hat{V}_c}{\mathrm{d}\hat{t}}\hat{l}_o + h_1\frac{\mathrm{d}\hat{\omega}}{\mathrm{d}\hat{t}}\hat{l}_o^2 + h_2\hat{\omega}^2\hat{l}_o^2 + h_4\hat{V}_c^2 + h_9\hat{\omega}\hat{l}_o\hat{V}_c\right) \tag{5}$$

where $\hat{\rho}_\infty$ is the external freestream density, g_0, g_1, g_4, g_9 and h_0, h_1, h_4, h_9 are nondimensional factors that depend on the store geometry, position, and orientation relative to the shear layer (exact expression given in Appendix B). Also, V_c is the store linear velocity (positive upwards) and ω is the rotational velocity (positive nose-up).

We next consider the effect of individual terms on the overall solution of Eq. (5). As a first step, we assume the linear velocity term (i.e., containing only $\hat{V}_c$) to be dominant. This can happen when the store is dropped with a large linear velocity and negligible angular velocity. In this case, the vertical motion of the store inside the cavity is given by Newton's second law, expressed as follows:

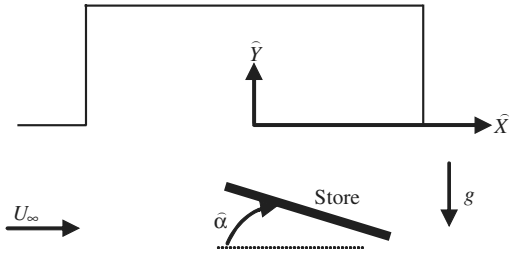

Fig. 2 Reference frame for the general problem of a slender axisymmetric store falling through a crossflow in the absence of viscosity and body forces.

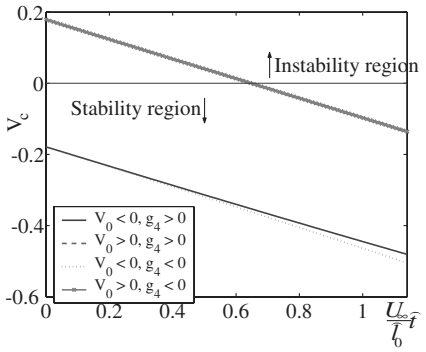

Fig. 3 Velocity of store while inside cavity for various drop conditions, with $V_c = \hat{V}_c/\delta U_\infty$. The values of parameters used are $|\hat{V}_0| = 0.18\delta U_\infty$ and $|g_4| = 0.75$.

$$\hat{m}_s \frac{\mathrm{d}\hat{V}_c}{\mathrm{d}\hat{t}} = \pi\hat{\rho}_\infty \delta \hat{l}_o^3 g_4 \hat{V}_c^2 - \hat{m}_s \hat{g}, \qquad \frac{\mathrm{d}\hat{Y}_c}{\mathrm{d}\hat{t}} = \hat{V}_c$$
$$\hat{I}_s \frac{\mathrm{d}\hat{\omega}}{\mathrm{d}\hat{t}} = \pi\hat{\rho}_\infty \delta \hat{l}_o^4 h_4 \hat{V}_c^2, \qquad \frac{\mathrm{d}\hat{\alpha}}{\mathrm{d}\hat{t}} = \hat{\omega} \tag{6}$$

where $\hat{m}_s$ and $\hat{I}_s$ are the mass and moment of inertia of the store about its axis, $\hat{g}$ is gravity, Y_c is the store c.g. position relative to the shear layer line (positive upwards) and $\hat{\alpha}$ is the angle between the store axis and the external freestream direction (positive clockwise). The store state (position, orientation, and velocity) is illustrated in Fig. 2. Also the factor g_4 does not vary significantly when the store is inside the cavity.

The following velocity expression can be obtained from this equation:

$$\hat{V}_c = -\sqrt{\frac{\hat{g}}{A}} \tanh\left(t\sqrt{\hat{g}A} + \frac{1}{2}\log\frac{\sqrt{\frac{\hat{g}}{A}} - \hat{V}_0}{\sqrt{\frac{\hat{g}}{A}} + \hat{V}_0} \right)$$
$$g_4 > 0 = -\sqrt{\frac{\hat{g}}{A}} \tan\left(t\sqrt{\hat{g}A} - \arctan\frac{\hat{V}_0}{\sqrt{\frac{\hat{g}}{A}}} \right), \qquad g_4 < 0 \tag{7}$$

where $A = \hat{\rho}_\infty \delta \hat{l}_o^3 g_4/\hat{m}_s$. Figure 3 shows a typical evolution of $\hat{V}_c$ while the store falls inside the cavity for various drop conditions given by $(\hat{Y}_0, \hat{\alpha}_0, \hat{V}_0, \hat{\omega}_0)$.

It is clear that irrespective of the signs of g_4 and $\hat{V}_0$, $\hat{V}_c$ eventually becomes negative inside the cavity. Although, if $\hat{V}_0 > 0$, then $\hat{V}_c$ stays positive for a certain time duration before turning negative. In other words, the inner volume of the cavity has a stabilizing influence on the store, in that it eventually falls towards the shear layer irrespective of $\hat{V}_0$. Also $h_4 > 0$ inside the cavity so that $\hat{\omega}$ and $\hat{\alpha}$ increase monotonically. These conclusions hold true for the cavity exhibiting negligible mean flow compared to the external crossflow. The influence of an appreciable mean flow can have a destabilizing effect on the store trajectory as seen in the analysis performed for a store falling in a subsonic medium [1].

If $\hat{\omega}$ terms in $\hat{F}$ are significant, a similar analysis can be done to find the drop conditions (i.e., $\hat{V}_0$ and $\hat{\omega}_0$) that would ensure that the store falls towards the shear layer. For example, if the store is dropped with very high $\hat{\omega}_0$ and low $\hat{V}_0$, the store may pitch up and move towards the cavity roof instead of the shear layer. The effect of the unsteady terms $\mathrm{d}\hat{V}_c/\mathrm{d}\hat{t}$ and $\mathrm{d}\hat{\omega}/\mathrm{d}\hat{t}$ can be similarly studied. However, it will be later seen that safe departure of the store can occur when it is dropped with a large linear velocity and a small angular velocity. Under this condition, the effect of the unsteady and $\hat{\omega}$ terms in Eq. (5) is considered small and hence not discussed further. More detailed analysis of the store trajectory inside the cavity has been given in [1] when the external flow is subsonic.

D. Force and Moment When Store Crosses Shear Layer

The general expressions for force and moment, when the store crosses the shear layer, are given in parametric form by

$$\hat{F} = \pi\hat{\rho}_\infty \delta \hat{l}_o^3 \Big(g_0 \frac{\mathrm{d}\hat{V}_c}{\mathrm{d}\hat{t}} \hat{l}_o + g_1 \frac{\mathrm{d}\hat{\omega}}{\mathrm{d}\hat{t}} \hat{l}_o^2 + g_2 \hat{\omega}^2 \hat{l}_o^2 + U_\infty^2 g_3 \hat{\alpha}^2 + g_4 \hat{V}_c^2 + U_\infty \delta g_5 \hat{\omega} \hat{l}_o + U_\infty^2 \delta g_6 \hat{\alpha} + U_\infty \delta g_7 \hat{V}_c + U_\infty g_8 \hat{\alpha}\,\hat{\omega}\,\hat{l}_o + g_9 \hat{\omega} \hat{l}_o \hat{V}_c + U_\infty g_{10} \hat{\alpha}\,\hat{V}_c + \delta^2 U_\infty^2 g_{11} \Big)$$
$$\hat{M} = \pi\hat{\rho}_\infty \delta \hat{l}_o^4 \Big(h_0 \frac{\mathrm{d}\hat{V}_c}{\mathrm{d}\hat{t}} \hat{l}_o + h_1 \frac{\mathrm{d}\hat{\omega}}{\mathrm{d}\hat{t}} \hat{l}_o^2 + h_2 \hat{\omega}^2 \hat{l}_o^2 + U_\infty^2 h_3 \hat{\alpha}^2 + h_4 \hat{V}_c^2 + U_\infty \delta h_5 \hat{\omega} \hat{l}_o + U_\infty^2 \delta h_6 \hat{\alpha} + U_\infty \delta h_7 \hat{V}_c + U_\infty h_8 \hat{\alpha}\,\hat{\omega}\,\hat{l}_o + h_9 \hat{\omega} \hat{l}_o \hat{V}_c + U_\infty h_{10} \hat{\alpha}\,\hat{V}_c + \delta^2 U_\infty^2 h_{11} \Big) \tag{8}$$

where $g_0, \ldots, g_{11}, h_0, \ldots, h_{11}$ are outlined in Appendix C. The effect of these loads is subsequently discussed in conjunction with the stage when the store is completely outside the cavity.

E. Force and Moment for Store Outside Cavity

When the store is completely outside the cavity, the resulting normal force and pitching moment on the store are expressed in a parametric form as follows, similar to Eq. (8):

$$\hat{F} = \pi\hat{\rho}_\infty \delta \hat{l}_o^3 \Big(g_0 \frac{\mathrm{d}\hat{V}_c}{\mathrm{d}\hat{t}} \hat{l}_o + g_1 \frac{\mathrm{d}\hat{\omega}}{\mathrm{d}\hat{t}} \hat{l}_o^2 + g_2 \hat{\omega}^2 \hat{l}_o^2 + U_\infty^2 g_3 \hat{\alpha}^2 + g_4 \hat{V}_c^2 + U_\infty \delta g_5 \hat{\omega} \hat{l}_o + U_\infty^2 \delta g_6 \hat{\alpha} + U_\infty \delta g_7 \hat{V}_c + U_\infty g_8 \hat{\alpha}\,\hat{\omega}\,\hat{l}_o + g_9 \hat{\omega} \hat{l}_o \hat{V}_c + U_\infty g_{10} \hat{\alpha}\,\hat{V}_c + \delta^2 U_\infty^2 g_{11} \Big)$$
$$\hat{M} = \pi\hat{\rho}_\infty \delta \hat{l}_o^4 \Big(h_0 \frac{\mathrm{d}\hat{V}_c}{\mathrm{d}\hat{t}} \hat{l}_o + h_1 \frac{\mathrm{d}\hat{\omega}}{\mathrm{d}\hat{t}} \hat{l}_o^2 + h_2 \hat{\omega}^2 \hat{l}_o^2 + U_\infty^2 h_3 \hat{\alpha}^2 + h_4 \hat{V}_c^2 + U_\infty \delta h_5 \hat{\omega} \hat{l}_o + U_\infty^2 \delta h_6 \hat{\alpha} + U_\infty \delta h_7 \hat{V}_c + U_\infty h_8 \hat{\alpha}\,\hat{\omega}\,\hat{l}_o + h_9 \hat{\omega} \hat{l}_o \hat{V}_c + U_\infty h_{10} \hat{\alpha}\,\hat{V}_c + \delta^2 U_\infty^2 h_{11} \Big) \tag{9}$$

where $g_0, \ldots, g_{11}, h_0, \ldots, h_{11}$ are now given in Appendix D.

To obtain more insight into this problem, we consider the following simplification. Because of the high speed of the external flow and because the store is inclined to the flow, the component of the external flow normal to the store is considered to be dominant compared to the store velocity. Hence when the store is external to the cavity, the dominant terms in $\hat{F}$ and $\hat{M}$ contain $\hat{\alpha}$. Next, we linearize the dominant terms about $\hat{\alpha} = 0$ to get

$$\hat{F} = \pi\delta^2 \hat{l}_o^3 \beta f(\hat{\alpha}), \qquad \hat{M} = \pi\delta^2 \hat{l}_o^4 \beta f_m(\hat{\alpha}), \qquad \beta = \hat{\rho}_\infty U_\infty^2$$
$$f(\hat{\alpha}) = g_6 \hat{\alpha}, \qquad f_m(\hat{\alpha}) = h_6 \hat{\alpha} \tag{10}$$

Using Eq. (10) and following Eq. (6), the governing equation for the store trajectory outside the cavity becomes

$$\hat{m}_s \frac{\mathrm{d}\hat{V}_c}{\mathrm{d}\hat{t}} = \pi\hat{\rho}_\infty U_\infty^2 \delta^2 \hat{l}_o^3 g_6 \hat{\alpha} - \hat{m}_s \hat{g}, \qquad \frac{\mathrm{d}\hat{Y}_c}{\mathrm{d}\hat{t}} = \hat{V}_c$$
$$\hat{I}_s \frac{\mathrm{d}\hat{\omega}}{\mathrm{d}\hat{t}} = \pi\hat{\rho}_\infty U_\infty^2 \delta^2 \hat{l}_o^4 h_6 \hat{\alpha}, \qquad \frac{\mathrm{d}\hat{\alpha}}{\mathrm{d}\hat{t}} = \hat{\omega} \tag{11}$$

After the store exits the shear layer, let its state be denoted by $(\hat{Y}_1, \hat{\alpha}_1, \hat{V}_1, \hat{\omega}_1)$. When $\hat{\alpha}_1$ is large, because $g_6 > 0$ in Eq. (11), the linear dependence of $f(\hat{\alpha})$ on $\hat{\alpha}$ results in large $\hat{F}$. This increases the likelihood of $\hat{F}$ to overcome gravity and the store to return back toward the cavity. This is further demonstrated from the expression for $\hat{V}_c$ which is obtained by solving Eq. (11) with $\hat{V}_1$ as the initial condition. As a result we get

$$\hat{V}_c = B(-\hat{\omega}_1 \cos\Lambda\hat{t} + \Lambda\hat{\alpha}_1 \sin\Lambda\hat{t}) - \hat{g}\,\hat{t} + B\hat{\omega}_1 + \hat{V}_1 \tag{12}$$

where $\Lambda^2 = \pi\hat{\rho}_\infty U_\infty^2 \delta^2 \hat{l}_o^4 |h_6|$, $B = \hat{I}_o g_6/|h_6|$. The linear velocity expression consists of a sinusoidal term, a linear term, and an offset. From an order of magnitude analysis, it can be shown that the offset term is the dominant one. For a given $(\hat{Y}_1, \hat{\alpha}_1)$, if

$$\frac{\hat{\omega}_1}{\hat{V}_1} > -\frac{1}{B} \tag{13}$$

then $\hat{V}_c$ becomes positive when

$$\frac{1}{\Lambda}\arccos\left(1 + \frac{\hat{V}_1}{B\hat{\omega}_1}\right) < \hat{t} < \frac{2\pi}{\Lambda} - \frac{1}{\Lambda}\arccos\left(1 + \frac{\hat{V}_1}{B\hat{\omega}_1}\right)$$

The implication is that over this time interval, the store returns toward the cavity. The above discussions indicate that the store dynamics outside the cavity can be characterized by a stable region with linear boundary, where a stable region is defined as the set of $(\hat{Y}_1, \hat{\alpha}_1, \hat{V}_1, \hat{\omega}_1)$ such that the store exhibits a safe drop.

The stability analysis performed so far, particularly Eq. (13), is based on the simplified dynamics of the store. This is given in Eq. (11) under the assumption that the $\hat{\alpha}$ terms are dominant. To verify if this stability boundary is valid in general, we evaluate the more detailed model given by Eq. (9) together with Newton's second law to predict the conditions $(\hat{V}_1, \hat{\omega}_1)$ that result in an unsafe store departure for a particular $(\hat{Y}_1, \hat{\alpha}_1)$. This is shown in Fig. 4 and independently validates the linear stability boundary predicted above. Hence it was not felt necessary to discuss the store dynamics further in the case where terms other than $\hat{\alpha}$ are dominant.

F. Comparison of Shear Layer Structures and Store Motion Induced Potential

In this section, we study the relative contributions of the wavy shear layer profile and the store motion induced potential to the normal force and pitching moment. For this, we assume the simplified load expression for the store when it is completely outside the cavity, as illustrated in Eq. (10). For the wavy shear layer, we use Eq. (4). Then we have

$$\frac{|\hat{F}_w|}{|\hat{F}|} \sim \underbrace{\frac{\mu\delta_s}{\delta}}_{I} \underbrace{\frac{(\hat{\rho}_\infty U_\infty^2)_r}{\hat{\rho}_\infty U_\infty^2}}_{II} \underbrace{\frac{\max_i(W_i\lambda_i^2)G_0}{g_6\alpha}}_{III} \tag{14}$$

The second and third terms are of the order of 1. Therefore, if $\frac{\mu\delta_s}{\delta}$ is small, which is henceforth referred to as the thin shear layer, its effect on the store loads is negligible. On the other hand, if $\frac{\mu\delta_s}{\delta}$ is of the order of unity, which is henceforth referred to as the "thick" shear layer, its effect on the store loads cannot be neglected.

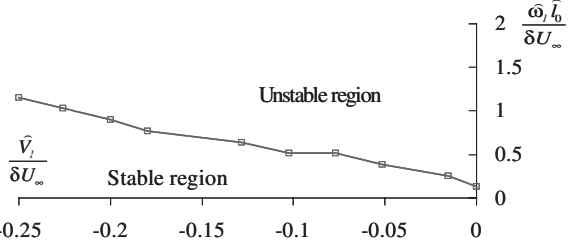

Fig. 4 Stability region predicted by the outside-cavity model in the no-control case. The initial conditions for the model are $Y_1 = (\hat{Y}_1/\delta\hat{l}_o) = -1.63$ and $\alpha_1 = (\hat{\alpha}_1/\delta) = 0.01$ with $V_1 = \hat{V}_1/\delta U\infty$ and $\omega_1 = \hat{\omega}_1\hat{l}_o/\delta U\infty$ shown in the plot. The uncertainty in the stability boundary is as follows: $\Delta V_1 = \pm 0.005$, $\Delta\omega_1 = \pm 0.125$. The crossflow Mach number is 2.46, the Reynolds number based on store length is 4.9×10^6, the cavity aspect ratio is 5, and the store length is half of the cavity length.

III. Analysis of the Complete Store Drop

The low-order model developed in Secs. II.C–II.E is now used to analyze the store trajectory as it is dropped from inside the cavity to the point where it has either exhibited successful drop or it starts to return back into the cavity. This analysis is performed for two cases: 1) when microjets are off, and 2) when the microjets are switched on. Finally, a store drop model extension that considers the wavy shear layer profile at the cavity opening is discussed at the end of this section.

A. No Microjets Present

Let the store be dropped from inside the cavity with the conditions $(\hat{Y}_0, \hat{\alpha}_0, \hat{V}_0, \hat{\omega}_0)$, with $\hat{\alpha}_0$ positive and small, $\hat{V}_0 < 0$, and $\hat{\omega}_0 > 0$ but not large enough so that the store hits the cavity roof immediately. It follows from Sec. II.C that $\hat{\omega}$, $\hat{\alpha}$, and $|\hat{V}_c|$ inside the cavity increase monotonically by the time they reach the shear layer. Also, from Eqs. (6) and (10), it follows that when the store crosses the shear layer, the portion of the store inside the cavity experiences a normal force proportional to $\hat{V}_c^{\,2}$ while the portion outside experiences a force proportional to $f(\hat{\alpha})$. The latter is considered dominant because of the high external flow speed. Now from Eq. (10) (with $h_6 < 0$) and from the fact that the tail side is first exposed to the external stream when the store exits the cavity, it follows that there is an increase in $\hat{M}$ in the nose-down (negative) direction and a consequent decrease in $\hat{\omega}$. Despite this, if the store is released with a large $\hat{\omega}_0$ when compared to $\hat{V}_0$, then $\hat{\omega}_1$ is large when the store exits the cavity and Eq. (13) is satisfied, thus implying an unsuccessful drop. It also follows that if the store is released with a small $\hat{\omega}_0$, then $\hat{\omega}_1$ is small and Eq. (13) is not satisfied. In that case, the store exhibits a clean departure. In summary, if the store is dropped with a small $\hat{\omega}_0$ when compared to $\hat{V}_0$ (see Fig. 4), the store is predicted to exhibit a safe departure from inside the cavity. The case where the nose is first exposed to external flow, when the store crosses the shear layer, can be similarly analyzed and has not been pursued hereafter.

B. Microjets Present

Next we analyze the store drop phenomenon when microjets are switched on. The following dominant effects are observed due to the introduction of microjets: 1) flow deceleration ($\hat{U}_{\infty,2}/\hat{U}_{\infty,1} < 1$), 2) flow compression ($\hat{\rho}_{\infty,2}/\hat{\rho}_{\infty,1} > 1$), 3) flow turning (away from the cavity by an angle θ), and 4) introduction of plane shock waves at the cavity leading edge. Figure 5 gives a pictorial description of these

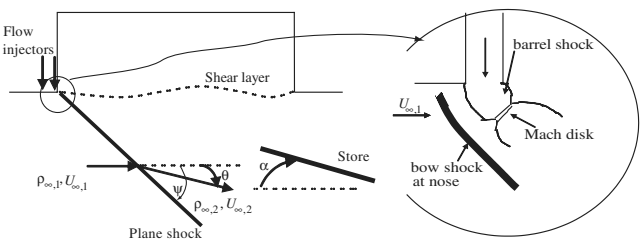

Fig. 5 Shock geometry outside the cavity due to application of microjet-based flow injectors at the leading edge and upstream end.

effects. As illustrated here, the shock is initially normal because of transverse injection and then turns toward the cavity a few jet diameters in the downstream direction. Because the ratio of microjet diameter to the cavity length is of the order of 0.001, the normal shock is very small compared to the oblique portion. The shock angle is measured from the leading edge to about 40% of the cavity length in the downstream direction. Refer to [9] for more details.

Because the store is released in the middle of the cavity, it is not expected to intersect the plane shock line; therefore effect 4) is not directly considered any further in the discussions below. However, effects 1)–3) influence $\hat{F}$ and $\hat{M}$ on the store and their magnitudes are determined by the ratio of microjet-crossflow momentum ratio C_μ defined below*:

$$C_\mu = \frac{(\rho A U^2 N)_\mu}{\frac{1}{2}(\rho U^2)_\infty (\hat{D}_o \delta_{BL})} \tag{15}$$

The dependence of effects 1)–3) on C_μ was experimentally determined in the Florida State University (FSU) setup and is explained in Appendix A. The main idea is twofold: a) the flow visualization studies done using the FSU cavity setup established the C_μ dependence of the shock orientation angle ψ and θ (Fig. 5), and b) the effects 1)–3) were quantified using the results of a) and plane shock theory [10]. The resulting dependence of 1)–3) on C_μ is given in Fig. 6. It should be noted that all these effects are introduced when the store exits the cavity, whereas they do not affect the mean flowfield inside the cavity.

Now $\hat{F}$ and $\hat{M}$ have been derived and analyzed in Sec. II for general values of $\hat{\rho}_\infty$ and U_∞. To study the effect of microjets, we vary C_μ, which in turn introduces the changes 1)–3). This in turn changes $\hat{F}$ and $\hat{M}$ as outlined in Sec. II. An important point to note here is the change in $\hat{F}$ and $\hat{M}$ as a function of θ. In Fig. 7, the responses of $\hat{F}$ and $\hat{M}$ as a function of time and as θ is varied, are illustrated. It is clear from the figure that a dramatic change in the slope of $\hat{M}$ occurs when θ is increased. In particular, $\hat{M}$ becomes negative when θ is below a certain value and positive for a higher value of θ, which essentially indicates onset of the store returning toward the cavity, as explained later. A similar trend is observed for $\hat{F}$. It should also be noted that the variations of $\hat{F}$ and $\hat{M}$ with effects 1) and 2) are more gradual. Another noteworthy point is that Fig. 7 shows a sharp change in $\hat{F}$ and $\hat{M}$ when the store moves from inside the cavity to the shear layer region, irrespective of the value of θ. The reason is due to modeling of the shear layer as a line of separation between the no-flow inside-cavity region and the external crossflow region. For operating conditions similar to those considered in this paper, the mean internal flow was not more than 10% of the external stream near the upstream half of the cavity and less than 20% near the downstream half [9]. Hence the mean internal flow can be neglected for store drops near the cavity middle. The effect of an appreciable mean flow inside the cavity is a topic of ongoing investigation being done along the lines of Shalaev et al. [1].

To further analyze the dependence of $\hat{M}$ on θ, we consider the general expression for $\hat{M}$ given by Eq. (8) when the store crosses the shear layer. We consider the following dominant terms in the equation. In Sec. II.C, the linear velocity component in force and moment expressions was considered to be dominant inside the cavity under specific store drop conditions. Also in Sec. II.E, the terms containing the angle of attack of the store were considered to be dominant in the force and moment expressions. So when the store crosses the shear layer, it is assumed that all the above terms are significant. Also because of the importance of angle of attack terms

*The subscript μ refers to the mean microjet properties at the microjet nozzle exit, subscript ∞ refers to the mean undisturbed external flow properties, ρ and U are the mean dimensional density and flow speed, A is the microjet cross-section area, N is the number of microjets, $\hat{D}_o$ is the cavity width as shown in Fig. E1 (in Appendix E), and δ_{BL} is the dimensional boundary layer thickness at the cavity leading edge. Also, $(\rho U^2)_\mu$ depends on the pressure at which the microjets are activated, thereby establishing a direct relationship between the microjet pressure and C_μ.

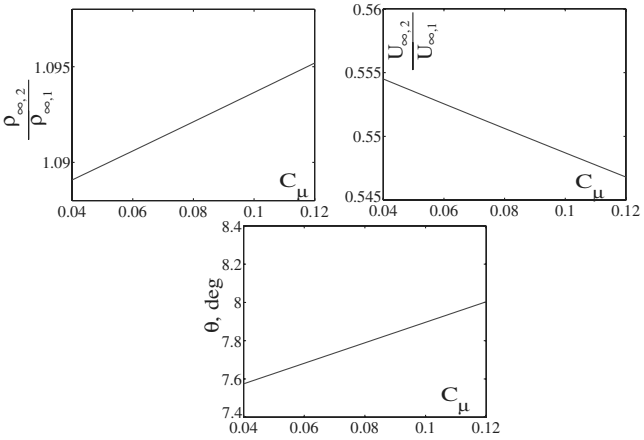

Fig. 6 Variation of external flow properties with C_μ due to the application of microjets.

outside the cavity and linear velocity terms inside the cavity, we also consider the product of linear and angular velocity (which is time rate of change of angle of attack) terms in the force and moment expressions to be significant. In this case, we have

$$\hat{M} = \pi \hat{\rho}_\infty \delta \hat{l}_o^4 \Big[\underbrace{h_4 \hat{V}_c^2}_{I} + \underbrace{h_9 \hat{\omega} \hat{l}_o \hat{V}_c}_{II} + \underbrace{U_\infty^2 h_3 (\hat{\alpha} - \theta)^2}_{III} + \underbrace{U_\infty^2 \delta h_6 (\hat{\alpha} - \theta)}_{IV} \Big] \tag{16}$$

These terms are plotted in Fig. 8. Please note that both Eq. (16) and Fig. 8 are valid at the short time interval indicated in the figure when the initial transition between the internal and external cavity flows takes place. It is clear that in the region of interest, when the store touches the shear layer from inside the cavity, the dominant effect is the change in sign of terms II and IV in $\hat{M}$. In spite of the assumption mentioned above Eq. (16), term III can be observed to be negligible. In addition, the region of interest circled in the figure shows that term I remains negative after the transition to the outside takes place. Term II changes sign because of change in sign of h_9 which represents relative contributions of the portions of the store completely immersed, partially immersed, and completely outside the cavity. As such, these dynamic variations in h_9 are dependent on the initial store drop conditions but not directly on the control variable (C_μ). The more interesting observation is that the sign of term IV depends on $\hat{\alpha} - \theta$ (it can be checked that h_6 does not vary strongly in sign). Because of these features, a drastic change in $\hat{M}$ can be observed at the instant when the store hits the shear layer. At this point, if $\hat{\alpha}$ is greater than θ, there is a negative pitching moment because the store tail is exposed to the external flow. However, if θ is increased by introducing higher microjet pressures such that $\hat{\alpha}$ becomes less than θ at this point, then there exists a value for θ beyond which the pitching moment on the store becomes positive.

It follows that when the microjets are switched on such that θ is less than a certain value, $\hat{M}$ increases in the negative direction and causes $\hat{\omega}$ to decrease when the store crosses the shear layer. At this point, Eq. (13) is not satisfied which implies that the store exhibits a safe drop. When microjet pressures are increased, there is a further increase in θ. If θ exceeds the limiting value, $\hat{M}$ increases positively and corresponding $\hat{\omega}$ increases when the store crosses the shear layer. An increase in $\hat{\omega}_1$ causes Eq. (13) to be satisfied leading to an unsuccessful drop. Also this trend is independent of $\hat{\omega}_0$, as long as the latter is not too high to overwhelm $\hat{F}$ and $\hat{M}$ when compared to the other terms. The variation of the store state as it crosses the shear layer in the absence and presence of microjets is given in Fig. 9.

In summary, the introduction of microjets is predicted to ensure safe departure for any $\hat{\omega}_0$ as long as θ is less than a certain value (see Fig. 8). However, for θ greater than this limit, which occurs for large microjet pressures, the store is predicted to return back to the cavity.

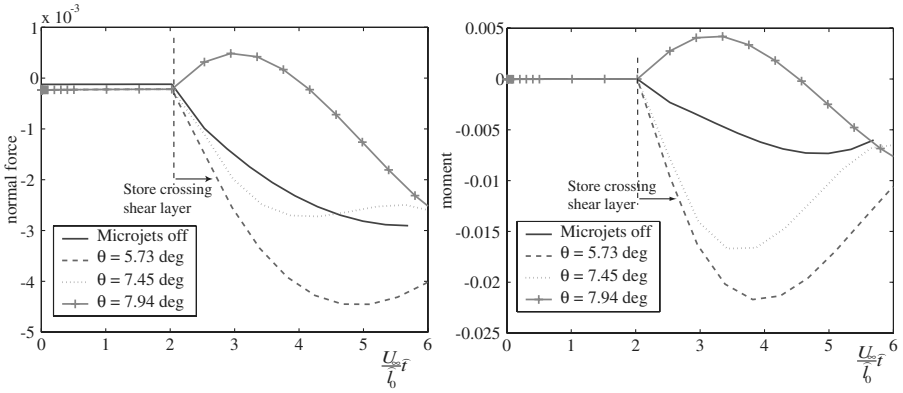

Fig. 7 Model-predicted $\hat{F}$ and $\hat{M}$ evolution with time for different θ when the store passes through the shear layer. The other external flow parameters used are $\hat{\rho}_{\infty,2}/\hat{\rho}_{\infty,1} = 1.818$, and $\hat{U}_{\infty,2}/\hat{U}_{\infty,1} = 0.915$. Also, the crossflow uncontrolled Mach number is 2.46, the Reynolds number based on store length is 4.9×10^6, the cavity aspect ratio is 5, and the store length is half the cavity length. A smoothing function is used to remove noise in the force and moment predictions of the model.

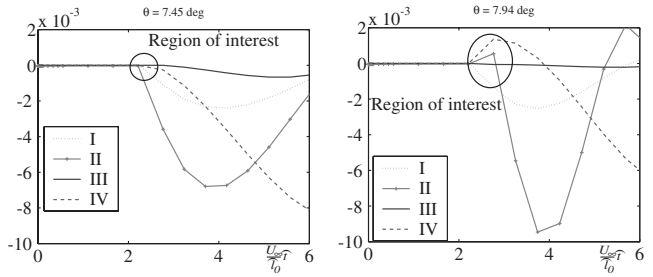

Fig. 8 Different components of the model-predicted $\hat{M}$ [from Eq. (16)] and their evolution with time for different θ when the store passes through the shear layer. The other external flow parameters used are $\hat{\rho}_{\infty,2}/\hat{\rho}_{\infty,1} = 1.818$, and $\hat{U}_{\infty,2}/\hat{U}_{\infty,1} = 0.915$. Also, the crossflow uncontrolled Mach number is 2.46, the Reynolds number based on store length is 4.9×10^6, the cavity aspect ratio is 5, and the store length is half of the cavity length. A smoothing function is used to remove noise in the moment prediction of the model.

C. Model Extension

In previous sections, we discussed the store drop trajectory when the shear layer at the cavity opening is considered thin. In Sec. III.C.1, we extend the store drop model to include the effect of the wavy shear layer profile on the store drop trajectory. In Sec. III.C.2, this extension is further used to study the effect of the drop location of the store inside the bay on its trajectory.

1. *Effect of Thick Shear Layer*

When the shear layer is thick, we cannot discount the effect of the wavy shear layer profile on the store $\hat{F}$ and $\hat{M}$. In this case, we use the technique developed in Sec. II.A for estimating the effect of the shear layer profile on the store $\hat{F}$ and $\hat{M}$. The latter are parameterized as given in Eq. (5) and the detailed expressions of $\hat{F}$ and $\hat{M}$ are given in Appendix D. The unknown in these expressions is the shear layer profile. In this paper, the shear layer profile was obtained from flow visualization experiments conducted on a rectangular cavity of aspect ratio 5.1 under Mach 2.0 flow in the FSU wind tunnel facility [9]. The mean flowfield inside and around the cavity was recorded for different microjet pressures (or equivalently, for different values of C_μ) using the technique of particle image velocimetry (PIV). From the mean flowfield, the shear layer profile was identified. The specific shear layer profile for the FSU cavity is shown in Fig. 10. Large scale vortical structures are observed in the uncontrolled shear layer; when microjets are switched on, these structures disappear, leading to a different shear layer profile, as illustrated in Fig. 10.

Using the experimental data shown in Fig. 10, we can obtain the shear layer profile for any arbitrary C_μ by interpolation. The effect of shear layer thickness is examined by comparing the model predictions to experimental results in Sec. IV.C.

It should be noted that the aforementioned model extension pertains to only the shear layer thickness. Because the Strouhal number associated with the unsteady effects such as the acoustic waves inside the cavity and the convective shear layer waves is typically much higher than that associated with the store motion for the flow conditions covered in this paper, these unsteady effects are ignored. The case where the Strouhal numbers are comparable has been further discussed by Malmuth [11] and is a subject of ongoing investigation.

2. *Effect of Initial Drop Location of Store Inside Bay*

The interesting point to note from Fig. 10 is that the shear layer thickness not only varies with change in C_μ but also with the

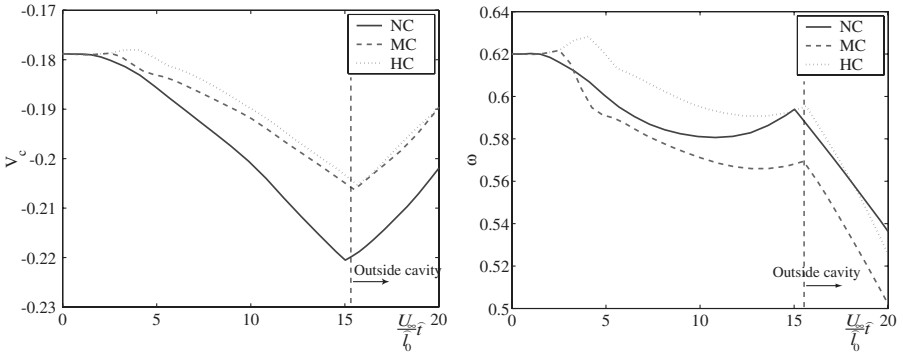

Fig. 9 $\hat{V}_c$ and $\hat{\omega}$ evolution with time for different control inputs when the store passes through the shear layer. The control inputs are specified in Table 1 and are classified as follows: 1) no control (NC), 2) microjet control on (MC), and 3) high microjet pressure control (HC). Also, the crossflow uncontrolled Mach number is 2.46, the Reynolds number based on store length is 4.9×10^6, the cavity aspect ratio is 5, and the store length is half of the cavity length.

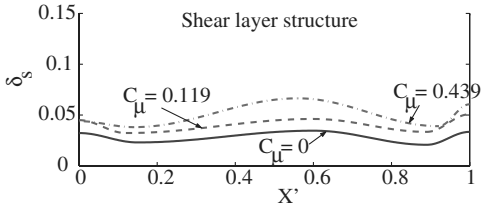

Fig. 10 Shear layer profile for different microjet momentum ratios, obtained from FSU flow visualization studies [9]. In addition, the flow conditions for the FSU setup are $M = 2.0$ and $Re = 3 \times 10^6$ (based on cavity length). Cavity dimension: $\hat{L}_o/\hat{W}_o = 5.1$.

streamwise location X'. The change in the shear layer thickness with X' causes nonuniformity in the flow outside the cavity that also varies with X'. Thus, the drop location of the store inside the cavity is expected to change its trajectory. This change can be estimated using the model extension developed in Sec. III.C.1 and is discussed in more detail in Sec. IV.C where the model predictions are compared with experimental results. In particular, the change in the store trajectory is studied when the store is dropped from 1) near the leading edge of the cavity ($X'_c = 0.4$), 2) near the middle of the cavity ($X'_c = 0.58$), and 3) near the trailing edge ($X'_c = 0.76$). Here, X'_c refers to the store c.g. streamwise coordinate.

The above study is limited by the assumptions that the store does not intersect the plane shock waves due to the microjets during its drop, and that the streamwise coordinate of the store is not changed during its motion. In the former case, the diffractive effects associated with the shock-line-store intersection are ignored while the latter assumption is made because the streamwise motion of the store during its drop is insignificant compared to the transverse motion and therefore the streamwise drag force on the store is not considered in this paper. In addition, the effect of interaction of the shock waves associated with the store (when it is outside the cavity) with the shear layer or with shock waves associated with the microjets is ignored. The rationale is that the shock waves associated with the store are considered to be negligibly weak because of the slender body geometry. However, these effects have been further discussed by Malmuth [11] and Bjorge et al. [12] and are also topics of ongoing investigation.

IV. Experimental Validation

In this section, we compare the low-order model predictions with results from experiments performed under the HIFEX Program [3–5].

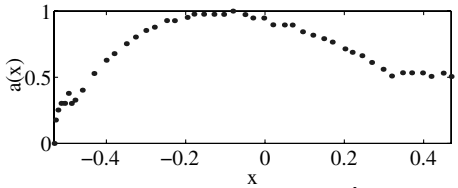

Fig. 11 Radius profile of the store. Here $x = \hat{x}/\hat{l}_o$ and $a = \hat{a}/\delta\hat{l}_o$. Also $x = 0$ corresponds to the store c.g.

Table 1 Changes in external flow properties with control. Three control inputs are considered: no control (NC), microjet control on (MC), and high microjet pressure control (HC). MC refers to 100–250 psig microjet pressure and HC refers to 200–250 psig microjet pressure. The first number here refers to the rows of microjets closest to the leading edge and the second number to the rows at the upstream end of the cavity. Also, the crossflow uncontrolled Mach number is 2.46, the Reynolds number based on store length is 4.9×10^6, the cavity aspect ratio is 5, and the store length is half of the cavity length

Item	NC	MC	HC	MC-NC, %	HC-MC, %
$\frac{\hat{\rho}_{\infty,2}}{\hat{\rho}_{\infty,1}}$	1.000	1.818	1.826	81.8	0.4
$\frac{\hat{U}_{\infty,2}}{\hat{U}_{\infty,1}}$	1.000	0.915	0.914	−8.5	−0.1
$\frac{\hat{\rho}_{\infty,2}\hat{U}^2_{\infty,2}}{\hat{\rho}_{\infty,1}\hat{U}^2_{\infty,1}}$	1.000	1.523	1.524	52.3	0.1
θ, deg	0	7.827	7.947	——	1.5

A. Experimental Details

A series of free drops of a slender axisymmetric store from a subscale generic weapons bay cavity was conducted under the HIFEX Program at various supersonic crossflow Mach numbers [3,5]. For brevity, this paper considers the experiments that were performed at two Mach numbers, 2.0 and 2.46. In addition, the bay model has the aspect ratio $\hat{L}_o/\hat{H}_o = 5$ and $\hat{L}_o/\hat{D}_o = 5$, with $\hat{H}_o$ being the depth and $\hat{D}_o$ the width of cavity. The Reynolds number of the flow based on the store length is approximately 4.9×10^6 and the speed of flow at Mach 2.46 is 579 m/s. The store is half the cavity length, its associated δ is 0.0615, and the store geometry is illustrated in Fig. 11. Moreover, the flow-injection actuator consists of two rows of sonic microjets along the leading edge and two rows near the upstream end of the cavity, situated about $\hat{L}_o/8$ distance from the leading edge. Here $\hat{L}_o$ is the cavity length, the microjets are of 400 μm in diameter, and each row consists of 50 microjets.

The store was dropped from $Y_c = (\hat{Y}_c/\delta\hat{l}_o) = 1.3$ from the middle of the cavity with nearly zero angle of attack and the store trajectory outside the cavity was recorded in high-speed video [3,5]. The drop tests were conducted using three different control inputs: no control (NC), microjet control on (MC), and high microjet pressure control (HC). Table 1 shows the changes in the external flow for the three control inputs and the store drop results are discussed later.

B. Comparison with the Model

The model-predicted trajectories are compared with experiments in Fig. 12. The figure shows unsafe store separation for the no-control and high microjet pressure cases and safe separation for the low microjet pressure case. The figure also indicates that the prediction of the experimental store trajectories by the low-order models is somewhat poor. One must note that the experimental trajectory shown here represents data from only one drop. It is likely that there is considerable variance associated with the store trajectory. Unfortunately, only a very limited number of experimental samples are available for comparison. Notwithstanding this observation, the quality of prediction of the model may be improved by considering diffractive effects associated with shock–shock interactions

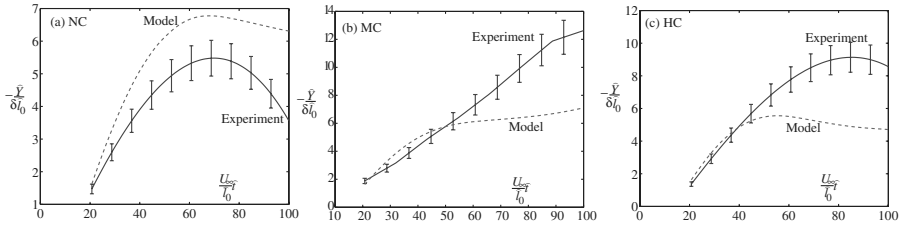

Fig. 12 Store trajectory prediction by the near-cavity model versus experimental observation for a) no control (NC), b) microjet control on (MC), and c) high microjet pressure control (HC). Also $(\hat{t}, \hat{Y}_c) = 0$ correspond to the instance when the store just exits the cavity from the middle of the bay, and increasing $-\hat{Y}_c$ corresponds to the store moving away from the bay. The crossflow Mach number is 2.46, the Reynolds number based on store length is 4.9×10^6, the cavity aspect ratio is 5, and the store length is half of the cavity length. The initial conditions for the model are given in Table 2.

Table 2 Initial conditions for the store trajectory analysis used in Fig. 12. The crossflow Mach number is 2.46, the Reynolds number based on store length is 4.9×10^6, the cavity aspect ratio is 5, and the store length is half of the cavity length

Item	Inside cavity (point 0)	While exiting cavity (point 1)
No control (NC)		
Y_c	1.30	−1.63
α	0.01	8.96
V_c	−0.18	−0.22
ω	0.62	0.59
Microjet control on (MC)		
Y_c	1.30	−1.63
α	0.01	9.10
V_c	−0.18	−0.22
ω	0.62	0.57
High microjet pressure control (HC)		
Y_c	1.30	−1.63
α	0.01	9.49
V_c	−0.18	−0.22
ω	0.62	0.60

mentioned in Sec. III: the shear layer thickness, and acoustic waves and mean flow inside the cavity. However the current model correctly predicts the variation of $\hat{Y}_c$ as the store drops outside the cavity. This in turn implies that the model accurately foretells whether the drop is successful or not under operating conditions similar to those considered in this paper. This indicates that despite the approximations invoked herein, the parameters considered in the model are sufficient in designing an optimal control strategy that ensures safe store departure.

To explain the behavior depicted in Fig. 12, we refer to Sec. III where we have analyzed the aerodynamic loads on the store for given drop conditions and microjet pressures. The point to note is that the store drop is successful when $|\hat{\omega}_1/\hat{V}_1|$ is small (see Fig. 4) and unsuccessful otherwise. When microjets are off and the store just exits the cavity, $\hat{\omega}_1$ is large because of large $\hat{\omega}_0$ at the drop point. The large $\hat{\omega}_1$ in comparison to $\hat{V}_1$ results in the store to exhibit an unsuccessful drop. When microjets are switched on, the external flow is compressed, decelerated, and turns away from the cavity with an angle θ. There exists a linear relationship between $\hat{M}$ and $\hat{\alpha} - \theta$ as soon as the store hits the shear layer such that $\hat{M}$ becomes negative when θ is small and positive when θ is large. In the case of MC, θ is small and the result is an increase in $\hat{M}$ in the negative direction and decrease in $\hat{\omega}$, when the store exits the cavity. Low $\hat{\omega}_1$ in comparison to $\hat{V}_1$ results in the store to exhibit a safe drop. When the microjet pressures are increased in the case of HC, θ exceeds the limiting value (Fig. 8). The result is that $\hat{M}$ and therefore $\hat{\omega}$ increase positively when the store crosses the shear layer. This results in large $\hat{\omega}_1$ in comparison to $\hat{V}_1$, thus leading to an unsuccessful drop. Figure 13

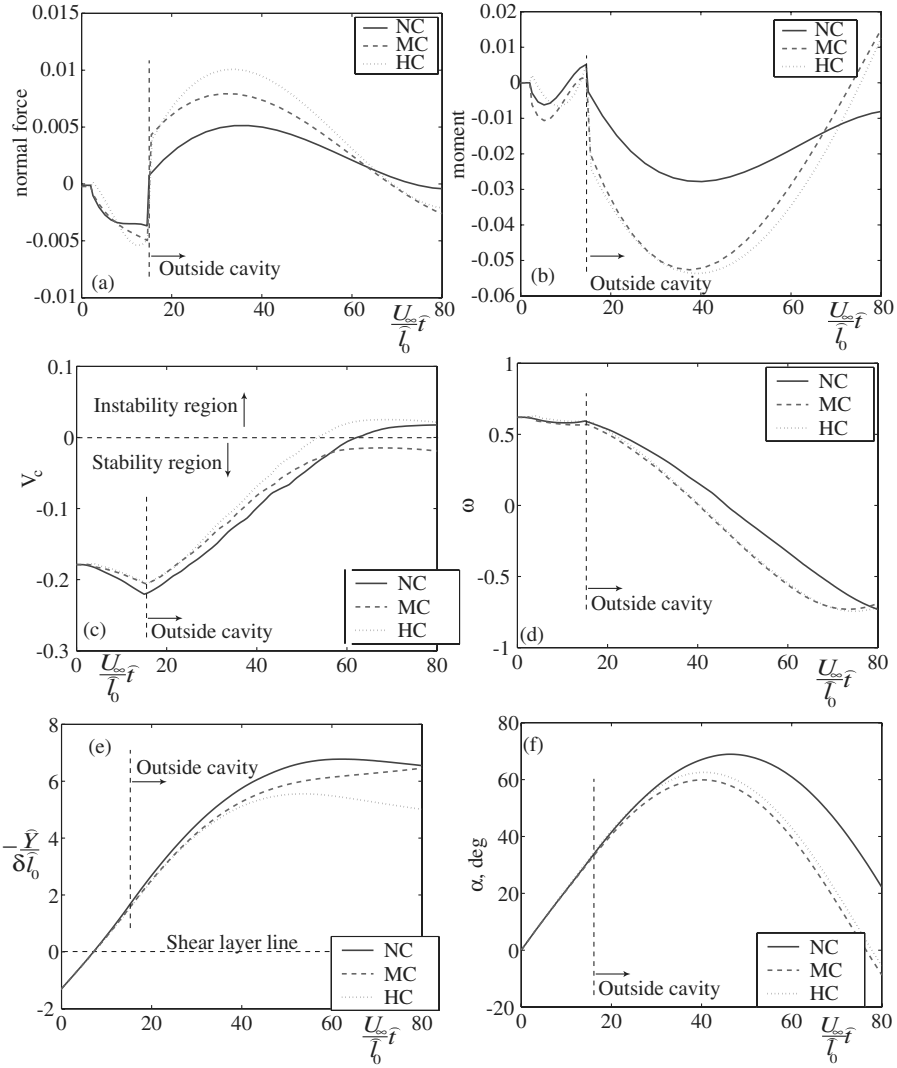

Fig. 13 Model-predicted normal force, pitching moment, and state of the store after being dropped from inside the cavity to when the store either returns back into the cavity or drops successfully in the three control cases: no control (NC), microjet control on (MC), and high microjet pressure control (HC). The crossflow Mach number is 2.46, the Reynolds number based on store length is 4.9×10^6, the cavity aspect ratio is 5, and the store length is half of the cavity length. The initial conditions are given in Table 2. A smoothing function is used to remove noise from force and moment predictions of the model.

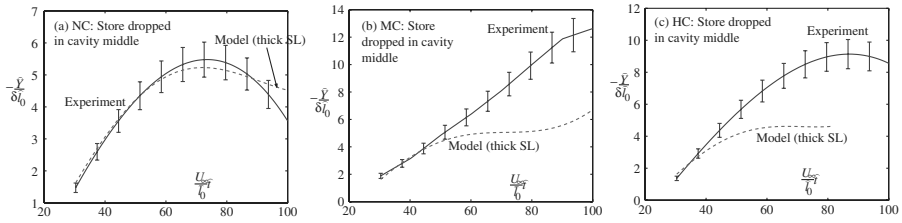

Fig. 14 Store trajectory prediction by the thick shear layer (SL) model versus experimental observation for a) no control (NC), b) microjet control on (MC), and c) high microjet pressure control (HC). Also $(\hat{t}, \hat{Y}_c) = 0$ correspond to the instance when the store just exits the cavity from the middle of the bay ($X'_c = 0.58$), and increasing $-\hat{Y}_c$ corresponds to the store moving away from the bay. The crossflow Mach number is 2.46, the Reynolds number based on store length is 4.9×10^6, the cavity aspect ratio is 5, and the store length is half of the cavity length. The initial conditions for the model are given in Table 3.

illustrates the force and moment as well as the state of the store after being dropped from inside the cavity to when the store either returns back into the cavity or drops successfully in the three control cases. It may be noted that in Fig. 13d, the difference in ω between HC and MC is not visibly apparent but is around 0.05. This leads to an appreciable change in α in Fig. 13f.

C. Comparison with Extended Model

In this section, we discuss the results of incorporating the thick shear layer wavy profile and the effect of the initial drop location of the store inside the bay on the store drop trajectory.

1. *Effect of Thick Shear Layer*

The thick shear layer model-predicted trajectories are compared with experiments in Fig. 14. The figure shows unsafe store separation for the no-control and high microjet pressure cases and safe separation for the low microjet pressure case, the initial drop conditions being similar in the three cases as illustrated in Table 3. Comparison of Figs. 12a and 14a shows that the store trajectory prediction of the no-control case is improved by including the thick shear layer profile. However, the quality of prediction of the MC and HC cases is unchanged by introduction of the shear layer thickness. One possible reason is that the shear layer profile near the leading edge becomes flatter (i.e., streamwise variation of the profile is small compared to unity) when microjet pressure is increased, as illustrated in Fig. 10. Also, from [11], it is clear that the presence of the shear layer profile at point $(X', Y' = 0)$ creates nonuniformity in the flow outside the cavity at point $(X' + \beta Y', Y')$, where $\beta^2 = M^2_{\infty,r} - 1$. In other words, the shear layer profile present near the leading edge affects the store trajectory when it is dropped near the middle of the cavity. The flatter profile resulting from higher microjet pressures diminishes the effect of the wavy shear layer profile on the store $\hat{F}$ and $\hat{M}$. In summary, the impact of the wavy profile is observable in the no-control case and not in the microjets-on cases.

Table 3 Initial conditions for the store trajectory analysis used in Fig. 14. The crossflow Mach number is 2.46, the Reynolds number based on store length is 4.9×10^6, the cavity aspect ratio is 5, and the store length is half of the cavity length

Item	Inside cavity (point 0)	While exiting cavity (point 1)
No control (NC)		
Y_c	1.30	−1.63
α	−44.27	33.58
V_c	−0.04	−0.16
ω	3.47	3.89
Microjet control on (MC)		
Y_c	1.30	−1.63
α	−43.27	35.43
V_c	−0.04	−0.19
ω	3.47	3.95
High microjet pressure control (HC)		
Y_c	1.30	−1.63
α	−43.27	32.58
V_c	−0.04	−0.17
ω	3.48	3.91

2. *Effect of Initial Drop Location of Store Inside Bay*

The model extension developed in Sec. III.C.1 allows us to study the effect of the initial drop location of the store inside the bay on its drop trajectory. The result is given in Figs. 14 and 15, with the initial drop conditions being similar in all the cases as illustrated in Tables 3 and 4. It is clear that when the store is dropped from near the leading edge of the bay, Fig. 15a shows unsafe store separation for the no-control case, and safe separation for the low and high microjet pressure cases. This is opposed to the store drop behavior when the store is released from the middle of the cavity (see Fig. 14), in which case store separation becomes unsafe with increase in microjet pressure. In the case when the store is dropped from near the trailing edge, the store makes a safe exit even in the absence of control, as shown in Fig. 15b. These predictions were corroborated by HIFEX experiments performed for the store drops near the leading, middle, and trailing edges of the bay. The resulting store trajectories were recorded in high-speed video; hence it should be noted that the corroboration is qualitative in nature.

V. Optimization of Control Input

The next step is to apply the aforementioned model to predict the optimal control input that would ensure a successful store drop. A suitable control parameter that can be optimized is the microjet momentum ratio C_μ as defined in Eq. (15). The optimal input is defined as the minimum value of C_μ which satisfies the user-specified microjet mass flow constraint and which guarantees safe release under a variety of drop conditions. For this purpose, the drop conditions from Table 2 were taken as the baseline and a combination of inside-cavity and outside-cavity models were used to determine whether the store exits the cavity successfully for different values of the control input, with the drops being performed from the cavity middle. The procedure was repeated for a different Mach number of external flow that was also tested under the HIFEX Program. The result is shown in Fig. 16.

It is clear that a general trend of successful drops at $C_\mu < 0.09$ and failed drops at $C_\mu > 0.09$ are predicted for both the Mach number cases. The successful drop at Mach 2.0 for $C_\mu = 0.08$ is qualitatively corroborated by a series of store drop experiments performed under the HIFEX Program [3,5]. It can also be observed that for Mach 2.0, a much smaller value of C_μ than that used experimentally suffices for ensuring a successful drop. However, for Mach 2.46, failure can occur for small C_μ and the optimal C_μ lies close to where the successful drop experiments were conducted. Once the optimal C_μ is determined, a suitable microjet-based actuator corresponding to this value of C_μ can be designed, which may be based on sonic or converging–diverging nozzles, the latter having the advantage of lower mass flux for the same momentum flux.

VI. Summary

Recent results obtained from the HIFEX Program [3–5] have demonstrated that successful store separation from a cavity under supersonic flow can be achieved by the introduction of an active control input. This input is applied using a tandem array of a microjet-based-transverse-fluid-injection system placed near the leading edge of the cavity. The current work postulates that the microjet-based

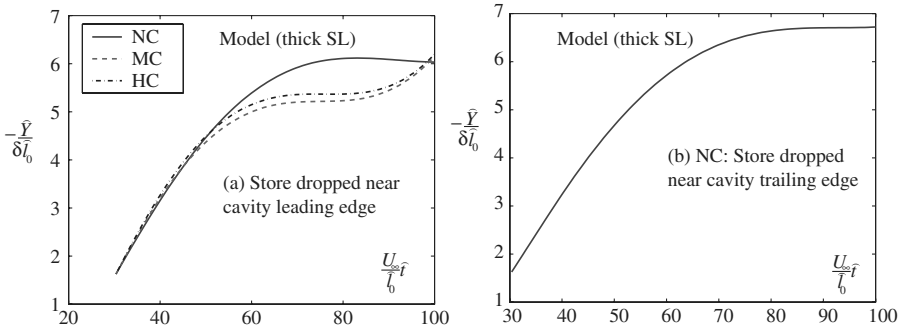

Fig. 15 Store trajectory prediction by the thick shear layer model when a) the store is dropped from near the leading edge ($X_c' = 0.4$), and b) the store is dropped from near the trailing edge ($X_c' = 0.76$), in the no control (NC), microjet control on (MC), and high microjet pressure control (HC) cases. Also $(\hat{t}, \hat{Y}_c) = 0$ correspond to the instance when the store just exits the cavity, and increasing $-\hat{Y}_c$ corresponds to the store moving away from the bay. The crossflow Mach number is 2.46, the Reynolds number based on store length is 4.9×10^6, the cavity aspect ratio is 5, and the store length is half of the cavity length. The initial conditions for the model are given in Table 4.

actuator modifies the flowfield near the cavity by modifying the shear layer and through the shock waves generated by the microjets, and thereby affects the store forces and moments.

This paper focuses on the development of a low-order model to predict the store trajectory under given drop conditions and control input. The model was used to predict the optimal control input to ensure a successful store departure using a given setup. The low-order model was developed based on the slender store geometry, thin shear layer at the cavity mouth, high Reynolds number external crossflow, plane shock waves associated with the microjets, and quiescent cavity. It may be noted that the shear layer profile and the cavity acoustic field are elements of a feedback loop; hence, by including the shear layer profile, the cavity acoustics are indirectly accounted for in the model. Also it was assumed that the tail was first exposed to the external stream when the store crosses the shear layer. The case where the nose is first exposed can be analyzed along similar lines.

The model was compared to the results of a series of store drop experiments performed under the HIFEX Program [3–5] at Mach 2.0 and 2.46 using a generic subscale weapons bay, with the store being dropped from the middle of the cavity. The trajectory information was obtained from high-speed video. Three observations were recorded: 1) the store drop was unsuccessful for the microjet-off case, 2) the store dropped safely when microjets were switched on, and 3) the store returned back to the cavity when the microjet pressures

Table 4 Initial conditions for the store trajectory analysis used in Fig. 15. The crossflow Mach number is 2.46, the Reynolds number based on store length is 4.9×10^6, the cavity aspect ratio is 5, and the store length is half of the cavity length

Item	Inside cavity (point 0)	While exiting cavity (point 1)
No control (NC): store dropped near cavity leading edge		
Y_c	1.30	−1.63
α	−44.27	23.64
V_c	−0.05	−0.17
ω	3.15	3.56
Microjet control on (MC): store dropped near cavity leading edge		
Y_c	1.30	−1.63
α	−43.27	22.33
V_c	−0.05	−0.18
ω	3.15	3.57
High microjet pressure control (HC): store dropped near cavity leading edge		
Y_c	1.30	−1.63
α	−43.27	21.01
V_c	−0.05	−0.19
ω	3.13	3.61
No control (NC): store dropped near cavity trailing edge		
Y_c	1.30	−1.63
α	−43.47	23.64
V_c	−0.05	−0.17
ω	3.13	3.56

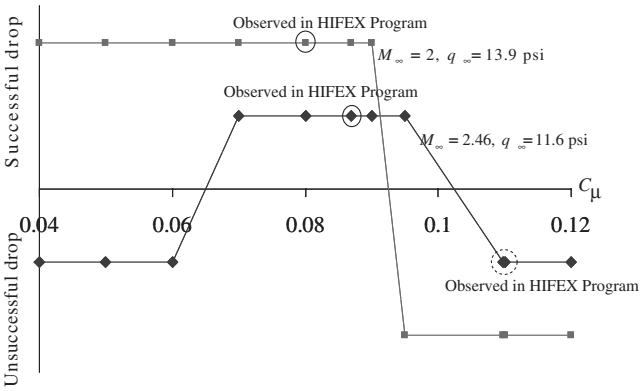

Fig. 16 Successful/unsuccessful store drop from cavity middle versus microjet momentum ratio C_μ. The model used corresponds to the thin shear layer one. The crossflow Mach number is 2.46, the Reynolds number based on store length is 4.9×10^6, the cavity aspect ratio is 5, and the store length is half of the cavity length. The drop conditions for this simulation are $Y_0 = 1.30$, $\alpha_0 = 0.01$, $V_0 = -0.18$, $\omega_0 = 0.62$, and $Y_1 = -1.63$.

were increased. These features were seen in the model as well. Although the model cannot exactly predict the store drop trajectory in part due to the many approximations that were made in developing the model, it can reliably predict the trend in the trajectory under operating conditions similar to those discussed in the paper. Most importantly, over the conditions examined, the model correctly predicts whether the store departure is safe or unsafe with and without microjet control.

This low-order model provides the following explanation for the experimental observations. The relevant points to be kept in mind are that a) $\hat{F}$ outside the cavity depends linearly on $\hat{\alpha}$ such that the store exits successfully if $|\hat{\omega}/\hat{V}_c|$ is small at the bay exit, and b) when the store passes through the shear layer, $\hat{M}$ depends linearly on $\hat{\alpha}$ which changes sign depending on the external flow turning angle θ. The reason for effect a) is that small $\hat{\omega}$ results in low $\hat{\alpha}$ and therefore $\hat{F}$ does not grow high enough to overcome gravity and the store falls out of the cavity safely. Because of high speed and no turning of the external flow in the no-control case, the main effect felt by the store is a). Thus, if the store is dropped with a large initial $\hat{\omega}$, it leaves the cavity with a large $\hat{\omega}$ in comparison to $\hat{V}_c$. This violates a) and results in an unsuccessful drop, confirming observation 1. On the other hand, if the drop condition is such that $\hat{\omega}$ is low in comparison to $\hat{V}_c$ when the store exits the cavity, the store will exhibit a safe drop.

With microjets on, the external flow turns away from the cavity. If the turning angle θ is less than a certain value, $\hat{M}$ increases in the negative direction. This results in a decrease in $\hat{\omega}$ as the store crosses the shear layer and satisfies effect a). Thus, the store exhibits a safe

drop, confirming observation 2. Higher microjet pressures cause a small increase in θ. If the flow turning angle exceeds the limiting value, $\hat{M}$ and consequently $\hat{\omega}$ increase in the positive direction, when the store crosses the shear layer. This violates a), leading to an unsuccessful drop and confirming observation 3.

The model is extended to include the effect of the wavy shear layer profile on the store trajectory. The extended model is then used to predict the store drop trajectory when it is released from near the leading edge, the middle, or the trailing edge of the bay. It is seen from both the extended model and the HIFEX experiments that when the store is released near the bay leading edge, the store drops unsafely in the no-control situation while it exhibits safe departure when microjets are switched on and even when microjet pressure is increased. When the store is dropped close to the trailing edge, it exhibits a safe departure and does not need any control.

Finally, the optimal control input to ensure clean store departure for a host of control inputs was found, with the drops being performed from the cavity middle. Expressed in terms of the microjet momentum ratio C_μ, the optimal control input was observed to match that used experimentally for certain flight conditions, and is predicted to be even smaller at other conditions. It may also be noted that the factors which were ignored in the development of the current model such as shock–shock interaction, acoustic waves, and mean flow inside the cavity are topics of current and future research.

Appendix A: Control Input as a Function of Microjet Pressure

The control action consists of the introduction of microjets near the leading edge of the cavity. After being introduced in the transverse direction, microjets turn and start mixing with the external crossflow, forming a virtual solid body. This obstruction to the crossflow leads to formation of shock waves near the cavity leading edge.

Empirically, the shock strength is governed by the microjet-to-external-flow momentum ratio [13]. To find the empirical relationship for a given microjet pressure profile, flow visualization experiments were conducted on a rectangular cavity of aspect ratio 5.1 under Mach 2.0 flow in the FSU wind tunnel facility [9]. This setup used 12 microjets of diameter 400 μm at the leading edge. To match the 12 microjet FSU setup with the HIFEX test [3,5], the momentum ratio parameter C_μ defined in Eq. (15) is used. The numerator in Eq. (15) is the mean momentum flux of all the active microjets while the denominator is the mean momentum flux of the external flow through the cross-section area of the virtual solid body formed by the microjets. The thickness of the body is the same as the penetration height of the microjets into the external flow and the latter is of the same order as the boundary layer thickness at the point of injection of microjets into the crossflow. Additionally, in Eq. (15), $\delta_{BL} \sim 0.015\hat{L}_o$ for the FSU cavity setup while for the HIFEX setup, $\delta_{BL} \sim 0.017\hat{L}_o$, where $\hat{L}_o$ is the cavity length as shown in Fig. E1 (in Appendix E).

The plane shock geometry resulting from introduction of microjets was studied for different momentum ratios using the FSU setup. The results are adapted from Zhuang et al. [9] and shown in Table A1. From this table, the shock geometry corresponding to an arbitrary C_μ can be determined by interpolation. Using the shock geometry and plane shock wave theory [10], the external flow properties (density, speed, and flow orientation) under the cavity can be determined.

Table A1 Plane shock geometry for different microjet momentum ratios (C_μ) corresponding to the FSU setup. External flow conditions: $M = 2.0$ and $Re = 3 \times 10^6$ (based on cavity length). Cavity dimension: $L/D = 5.1$

C_μ	0.119	0.306	0.573
Shock-to-freestream inclination angle	37	38	42
Angle θ (Fig. 5)	8	9	12

Appendix B: Expression for Forces and Moments on Store When Inside Cavity

When the store is inside the cavity, $\hat{F}$ and $\hat{M}$ expressions are given by Eqn. (5). Following the nondimensional scheme of Appendix E, we give below the expressions for g_0, g_1, g_4, g_9 and h_0, h_1, h_4, h_9 that are present in Eqn. (5). The expressions are given to accuracy $O(\frac{1}{256})$, where the small parameter is q.

$$g_0 = -\pi \int_{x_o}^{x_e} a(x)^2(2q^4 + 2q^6 + 1 - 2q^2)\,\mathrm{d}x$$

$$g_1 = \pi \int_{x_o}^{x_e} a(x)^2 x(2q^4 + 2q^6 + 1 - 2q^2)\,\mathrm{d}x$$

$$g_2 = 4\pi \int_{x_o}^{x_e} a(x)x^2(1 + q^2)(4q^8 + 8q^6 + 3q^2 - 1)q^3\,\mathrm{d}x$$

$$g_4 = \int_{x_o}^{x_e} \left(\frac{3}{16}a(x)^4 + \frac{1}{2}a(x)^2H^2 - H^4\right)\pi a(x)^4 - 4q^3(3q^2 - 1)(1 + q^2)\pi a(x)\,\mathrm{d}x$$

$$g_9 = \int_{x_o}^{x_e} \left(-\frac{3}{16}a(x)^4 - \frac{1}{2}a(x)^2H^2 + H^4\right)\pi x a(x)^4 + 32q^9(2q^2 + 1)(3q^2 - 2)(1 + q^2)\pi x a(x)\,\mathrm{d}x$$

$$h_0 = -\pi \int_{x_o}^{x_e} a(x)^2 x(2q^4 + 2q^6 + 1 - 2q^2)\,\mathrm{d}x \qquad \text{(B1)}$$

$$h_1 = \pi \int_{x_o}^{x_e} x^2 a(x)^2(2q^4 + 2q^6 + 1 - 2q^2)\,\mathrm{d}x$$

$$h_2 = 4\pi \int_{x_o}^{x_e} x^3 a(x)(1 + q^2)(4q^8 + 8q^6 + 3q^2 - 1)q^3\,\mathrm{d}x$$

$$h_4 = \int_{x_o}^{x_e} \left(\frac{3}{16}a(x)^4 + \frac{1}{2}a(x)^2H^2 - H^4\right)\pi x a(x)^4 - 4xq^3(2q^2 - 1)(1 + q^2)(12q^8 + 4q^6 - 2q^4 - q^2 + 1)\pi a(x)\,\mathrm{d}x$$

$$h_9 = \int_{x_o}^{x_e} \left(-\frac{3}{16}a(x)^4 - \frac{1}{2}a(x)^2H^2 + H^4\right)\pi x^2 a(x)^4 + 32q^9(2q^2 + 1)(3q^2 - 2)(1 + q^2)\pi x^2 a(x)\,\mathrm{d}x$$

$$q = \frac{a}{2H} = O\left(\frac{1}{2}\right)$$

Appendix C: Expression for Forces and Moments for Store Portion Partially Immersed in External Flow

When the store is passing through the shear layer, the contribution of the store portion inside the cavity to $\hat{F}$ and $\hat{M}$ is given in

Appendix B, while that of the portion outside the cavity is given in Appendix D [Eq. (D1)]. The contribution of the store portion partially immersed in external flow is given by Eq. (9) with $g_0, \ldots, g_{11}, h_0, \ldots, h_{11}$ given to accuracy $O(\frac{1}{256})$ below. The notation follows the nondimensional scheme of Appendix E.

$$g_0 = -\int_{x_1}^{x_2} a(x)^2[\Phi_1(n) + \Phi_p(m)]\,\mathrm{d}x$$

$$g_1 = \int_{x_1}^{x_2} a(x)^2 x[\Phi_1(n) + \Phi_p(m)]\,\mathrm{d}x$$

$$g_2 = \int_{x_1}^{x_2} x^2[a(x)P_1(x,t) - P_p(x,t)] + \frac{x^2 a(x)^2[\frac{\mathrm{d}}{\mathrm{d}m}\Phi_p(m) - \frac{\mathrm{d}}{\mathrm{d}n}\Phi_1(n)]}{\pi\sqrt{a(x)^2 - H^2}}\,\mathrm{d}x$$

$$g_3 = \int_{x_1}^{x_2} a(x)P_1(x,t)\,\mathrm{d}x$$

$$g_4 = \int_{x_1}^{x_2} a(x)P_1(x,t) - P_p(x,t) + \frac{a(x)^2[\frac{\mathrm{d}}{\mathrm{d}m}\Phi_p(m) - \frac{\mathrm{d}}{\mathrm{d}n}\Phi_1(n)]}{\pi\sqrt{a(x)^2 - H^2}}\,\mathrm{d}x$$

$$g_5 = \int_{x_1}^{x_2} a(x)\frac{\mathrm{d}a}{\mathrm{d}x}(x)x\left[\frac{a(x)\frac{\mathrm{d}}{\mathrm{d}n}\Phi_2(n)}{\pi\sqrt{a(x)^2 - H^2}} - P_{12}(x,t)\right] + \Phi_1(n)a(x)^2\,\mathrm{d}x + a(x_2)^2\Phi_1(n_2)x_2 - a(x_1)^2\Phi_1(n_1)x_1$$

$$g_6 = -\int_{x_1}^{x_2} a(x)\frac{\mathrm{d}a}{\mathrm{d}x}(x)P_{12}(x,t)\,\mathrm{d}x + a(x_2)^2\Phi_1(n_2) - a(x_1)^2\Phi_1(n_1)$$

$$g_7 = \int_{x_1}^{x_2} a(x)\frac{\mathrm{d}a}{\mathrm{d}x}\left[P_{12}(x,t) - \frac{a(x)\frac{\mathrm{d}}{\mathrm{d}n}\Phi_2(n)}{\pi\sqrt{a(x)^2 - H^2}}\right]\mathrm{d}x + a(x_1)^2\Phi_1(n_1) - a(x_2)^2\Phi_1(n_2)$$

$$g_8 = \int_{x_1}^{x_2} a(x)x\left[2P_1(x,t) - \frac{a(x)\frac{\mathrm{d}}{\mathrm{d}n}\Phi_1(n)}{\pi\sqrt{a(x)^2 - H^2}}\right]\mathrm{d}x$$

$$g_9 = 2\int_{x_1}^{x_2} x[P_p(x,t) - a(x)P_1(x,t)] + \frac{a(x)^2 x[\frac{\mathrm{d}}{\mathrm{d}n}\Phi_1(n) - \frac{\mathrm{d}}{\mathrm{d}m}\Phi_p(m)]}{\pi\sqrt{a(x)^2 - H^2}}\,\mathrm{d}x$$

$$g_{10} = \int_{x_1}^{x_2} a(x)\left[\frac{a(x)\frac{\mathrm{d}}{\mathrm{d}n}\Phi_1(n)}{\pi\sqrt{a(x)^2 - H^2}} - 2P_1(x,t)\right]\mathrm{d}x$$

$$g_{11} = a(x_1)^2\frac{\mathrm{d}a}{\mathrm{d}x}(x_1)\Phi_2(n_1) - \int_{x_1}^{x_2} a(x)\frac{\mathrm{d}a}{\mathrm{d}x}P_2(x,t)\,\mathrm{d}x - a(x_2)^2\frac{\mathrm{d}a}{\mathrm{d}x}(x_2)\Phi_2(n_2)$$

$$h_0 = -\int_{x_1}^{x_2} a(x)^2 x[\Phi_1(n) + \Phi_p(m)]\,\mathrm{d}x$$

$$h_1 = \int_{x_1}^{x_2} a(x)^2 x^2[\Phi_1(n) + \Phi_p(m)]\,\mathrm{d}x$$

$$h_2 = \int_{x_1}^{x_2} x^3[a(x)P_1(x,t) - P_p(x,t)] + \frac{x^3 a(x)^2[\frac{\mathrm{d}}{\mathrm{d}m}\Phi_p(m) - \frac{\mathrm{d}}{\mathrm{d}n}\Phi_1(n)]}{\pi\sqrt{a(x)^2 - H^2}}\,\mathrm{d}x$$

$$h_3 = \int_{x_1}^{x_2} xa(x)P_1(x,t)\,\mathrm{d}x$$

$$h_4 = \int_{x_1}^{x_2} x[a(x)P_1(x,t) - P_p(x,t)] + \frac{a(x)^2 x[\frac{\mathrm{d}}{\mathrm{d}m}\Phi_p(m) - \frac{\mathrm{d}}{\mathrm{d}n}\Phi_1(n)]}{\pi\sqrt{a(x)^2 - H^2}}\,\mathrm{d}x \tag{C1}$$

$$h_5 = \int_{x_1}^{x_2} x^2 a(x)\frac{\mathrm{d}a}{\mathrm{d}x}(x)\left[\frac{a(x)\frac{\mathrm{d}}{\mathrm{d}n}\Phi_2(n)}{\pi\sqrt{a(x)^2 - H^2}} - P_{12}(x,t)\right]\mathrm{d}x + x_2^2 a(x_2)^2\Phi_1(n_2) - x_1^2 a(x_1)^2\Phi_1(n_1)$$

$$h_6 = -a(x_1)^2\Phi_1(n_1)x_1 + a(x_2)^2\Phi_1(n_2)x_2 - \int_{x_1}^{x_2} \Phi_1(n)a(x)^2 - xa(x)\frac{\mathrm{d}a}{\mathrm{d}x}(x)P_{12}(x,t)\,\mathrm{d}x$$

$$h_7 = \int_{x_1}^{x_2} a(x)\left[a(x)\Phi_1(n) + x\frac{\mathrm{d}a}{\mathrm{d}x}(x)P_{12}(x,t)\right] - \frac{a(x)^2 x\frac{\mathrm{d}a}{\mathrm{d}x}(x)\frac{\mathrm{d}}{\mathrm{d}n}\Phi_2(n)}{\pi\sqrt{a(x)^2 - H^2}}\,\mathrm{d}x + a(x_1)^2\Phi_1(n_1)x_1 - a(x_2)^2\Phi_1(n_2)x_2$$

$$h_8 = \int_{x_1}^{x_2} 2x^2 a(x)P_1(x,t) - \frac{a(x)^2 x^2\frac{\mathrm{d}}{\mathrm{d}n}\Phi_1(n)}{\pi\sqrt{a(x)^2 - H^2}}\,\mathrm{d}x$$

$$h_9 = 2\int_{x_1}^{x_2} x^2[P_p(x,t) - a(x)P_1(x,t)] + \frac{a(x)^2 x^2[\frac{\mathrm{d}}{\mathrm{d}n}\Phi_1(n) - \frac{\mathrm{d}}{\mathrm{d}m}\Phi_p(m)]}{\pi\sqrt{a(x)^2 - H^2}}\,\mathrm{d}x$$

$$h_{10} = \int_{x_1}^{x_2} -2xa(x)P_1(x,t) + \frac{a(x)^2 x\frac{\mathrm{d}}{\mathrm{d}n}\Phi_1(n)}{\pi\sqrt{a(x)^2 - H^2}}\,\mathrm{d}x$$

$$h_{11} = \int_{x_1}^{x_2} -a(x)\left[\frac{\mathrm{d}a}{\mathrm{d}x}(x)\right]^2 P_2(x,t)x + a(x)^2\frac{\mathrm{d}a}{\mathrm{d}x}(x)\Phi_2(n)\,\mathrm{d}x + x_1 a(x_1)^2\frac{\mathrm{d}a}{\mathrm{d}x}(x_1)\Phi_2(n_1) - x_2 a(x_2)^2\frac{\mathrm{d}a}{\mathrm{d}x}(x_2)\Phi_2(n_2)$$

$$P_1(x,t) = -2.2n^5 + 8.9n^4 - 7.8n^3 - 2.8n^2 + 3.1n - 0.67$$

$$P_2(x,t) = 46,543.4n^3 - 11,980.9n^2 + 758.1n + \tfrac{\pi}{2}(n < 0.13)$$
$$= -7.8n^3 + 8.8n^2 + 0.91n - 0.35(n \geq 0.13)$$

$$P_{12}(x,t) = -10n^5 + 38n^4 - 36n^3 + 5n^2 - 0.66n + 0.19$$

$$P_p(x,t) = \sin(\pi m)\left[1 - \frac{1 + \pi m(1+2m^2)\cot(\pi m)}{6m^3}\right](n < 0.9)$$
$$= 501,427.6n^2 - 969,470.9n + 468,042.7(n \geq 0.9)$$

$$\Phi_1(n) = -23n^7 + 59n^6 - 27n^5 - 30n^4 + 28n^3 - 7.8n^2 + 0.071n + 2$$

$$\frac{d\Phi_1(n)}{dn} = -161n^6 + 354n^5 - 135n^4 - 120n^3 + 84n^2 - 15.6n + 0.071$$

$$\Phi_2(n) = 5.8n^5 - 28n^4 + 34n^3 - 9.6n^2 + 0.3n - 2.4$$

$$\frac{\mathrm{d}\Phi_2(n)}{\mathrm{d}n} = 29n^4 - 112n^3 + 102n^2 - 19.2n + 0.3$$

$$\Phi_p(n) = 23n^7 - 100n^6 + 160n^5 - 100n^4 + 6.9n^3 + 13n^2 + 0.12n - 0.0013$$

$$\frac{\mathrm{d}\Phi_p(n)}{\mathrm{d}n} = 161n^6 - 600n^5 + 800n^4 - 400n^3 + 20.7n^2 + 26n + 0.12$$

Here m, n are defined in [2].

Appendix D: Expression for Forces and Moments on Store When Outside Cavity

When the store is completely outside the cavity, the resulting $\hat{F}$ and $\hat{M}$ expressions are given by Eq. (9) with $g_0, \ldots, g_{11}, h_0, \ldots, h_{11}$ given to accuracy $O(\frac{1}{256})$ below. The notation follows the nondimensional scheme of Appendix E.

$$g_0 = -\int_{x_o}^{x_e} a^2(2q^4 + 6q^6 + 1 + 2q^2 + 16q^8)\,\mathrm{d}x$$

$$g_1 = \int_{x_o}^{x_e} a^2 x(2q^4 + 6q^6 + 1 + 2q^2 + 16q^8)\,\mathrm{d}x$$

$$g_2 = \int_{x_o}^{x_e} 4ax^2(6q^2 + 72q^6 + 3 + 15q^8 + 24q^4)q^3\,\mathrm{d}x$$

$$g_3 = \int_{x_o}^{x_e} 4a(15q^8 + 8q^6 + 1 + 2q^2 + 6q^4)q^3\,\mathrm{d}x$$

$$g_4 = \int_{x_o}^{x_e} 4a(6q^2 + 72q^6 + 3 + 15q^8 + 24q^4)q^3\,\mathrm{d}x$$

$$g_5 = \int_{x_o}^{x_e} (-4q^2)(-2 + 21q^6 + 6q^2)a\frac{\mathrm{d}a}{\mathrm{d}x}x + a^2(4q^8 + 2q^4 - 2q^2 + 2q^6 + 1)\,\mathrm{d}x + (-2q(x_e)^2 + 4q(x_e)^8 + 2q(x_e)^6 + 1 + 2q(x_e)^4)a(x_e)^2 x_e$$

$$g_6 = \int_{x_o}^{x_e} (-4q^2)(-1 + 3q^2)a\frac{\mathrm{d}a}{\mathrm{d}x}\,\mathrm{d}x + (-2q(x_e)^2 + 4q(x_e)^8 + 2q(x_e)^6 + 1 + 2q(x_e)^4)a(x_e)^2$$

$$g_7 = \int_{x_o}^{x_e} 4q^2(-2 + 21q^6 + 6q^2)a\frac{\mathrm{d}a}{\mathrm{d}x}\,\mathrm{d}x + (2q(x_e)^2 - 2q(x_e)^6 - 2q(x_e)^4 - 1 - 4q(x_e)^8)a(x_e)^2$$

$$g_8 = \int_{x_o}^{x_e} 8ax(3q^4 - 2 + 4q^2 + 9q^6 - 17q^8)q^3\,\mathrm{d}x$$

$$g_9 = -\int_{x_o}^{x_e} 8ax(-3 + 6q^4 - 17q^8 + 17q^6 + 6q^2)q^3\,\mathrm{d}x$$

$$g_{10} = -\int_{x_o}^{x_e} 8a(3q^4 - 2 + 4q^2 + 9q^6 - 17q^8)q^3\,\mathrm{d}x$$

$$g_{11} = -\int_{x_o}^{x_e} 2q(1 + 2q^4 - 2q^2)a\left(\frac{\mathrm{d}a}{\mathrm{d}x}\right)^2\mathrm{d}x - 2q(x_e)(-1 + 3q(x_e)^6 + q(x_e)^2)a(x_e)^2\frac{\mathrm{d}a}{\mathrm{d}x}\bigg|_{x_e}$$

$$h_0 = -\int_{x_o}^{x_e} a^2 x(4q^8 + 2q^4 - 2q^2 + 2q^6 + 1)\,\mathrm{d}x \qquad \text{(D1)}$$

$$h_1 = \int_{x_o}^{x_e} x^2 a^2(4q^8 + 2q^4 - 2q^2 + 2q^6 + 1)\,\mathrm{d}x$$

$$h_2 = \int_{x_o}^{x_e} 4x^3 a(-3 + 6q^4 - 17q^8 + 17q^6 + 6q^2)q^3\,\mathrm{d}x$$

$$h_3 = \int_{x_o}^{x_e} 4ax(2q^2 - 1 - 17q^8 + q^6)q^3 \,\mathrm{d}x$$

$$h_4 = \int_{x_o}^{x_e} 4ax(-3 + 6q^4 - 17q^8 + 17q^6 + 6q^2)q^3 \,\mathrm{d}x$$

$$h_5 = -\int_{x_o}^{x_e} 4q^2(-2 + 21q^6 + 6q^2)a\frac{\mathrm{d}a}{\mathrm{d}x}x^2 \,\mathrm{d}x + (-2q(x_e)^2 + 4q(x_e)^8 + 2q(x_e)^6 + 1 + 2q(x_e)^4)a(x_e)^2x_e^2$$

$$h_6 = \int_{x_o}^{x_e} (-4q^2)(-1 + 3q^2)a\frac{\mathrm{d}a}{\mathrm{d}x}x + (-1 + 2q^2 - 2q^4 - 2q^6 - 4q^8)a^2 \,\mathrm{d}x + (-2q(x_e)^2 + 2q(x_e)^4 + 2q(x_e)^6 + 4q(x_e)^8 + 1)a(x_e)^2x_e$$

$$h_7 = \int_{x_o}^{x_e} 4q^2(-2 + 21q^6 + 6q^2)a\frac{\mathrm{d}a}{\mathrm{d}x}x + a^2(4q^8 + 2q^4 - 2q^2 + 2q^6 + 1)\,\mathrm{d}x - (2q(x_e)^2 - 2q(x_e)^6 - 2q(x_e)^4 - 1 - 4q(x_e)^8)a(x_e)^2x_e$$

$$h_8 = \int_{x_o}^{x_e} 8ax^2(3q^4 - 2 + 4q^2 + 9q^6 - 17q^8)q^3 \,\mathrm{d}x$$

$$h_9 = -\int_{x_o}^{x_e} 8ax^2(-3 + 6q^4 - 17q^8 + 17q^6 + 6q^2)q^3 \,\mathrm{d}x$$

$$h_{10} = -\int_{x_o}^{x_e} 8ax(3q^4 - 2 + 4q^2 + 9q^6 - 17q^8)q^3 \,\mathrm{d}x$$

$$h_{11} = \int_{x_o}^{x_e} (-2q)(1 + 2q^4 - 2q^2)a\left(\frac{\mathrm{d}a}{\mathrm{d}x}\right)^2 x + 2q(q^2 - 1 + 3q^6)a^2\frac{\mathrm{d}a}{\mathrm{d}x}\,\mathrm{d}x + 2x_eq(x_e)(-q(x_e)^2 - 3q(x_e)^6 + 1)a(x_e)^2\frac{\mathrm{d}a}{\mathrm{d}x}\bigg|_{x_e}$$

Thick shear layer model: When the shear layer is thick, we cannot discount the effect of the wavy shear layer profile on the force and moment on the store. In this case, again assuming piecewise cosine components for the wavy profile as in Eq. (3), we get the different parameters of $\hat{F}$ and $\hat{M}$ expressions [given in Eq. (5)] as follows:

$$g_7 = -\frac{\beta\delta_s}{2\delta}\sum_i W_i\lambda_i^2[\cos(\lambda_i\{X_c^* + \beta Y_c^*\} + \zeta_i)k_{c,i} + \sin(\lambda_i\{X_c^* + \beta Y_c^*\} + \zeta_i)k_{s,i}]$$

$$h_7 = -\frac{\beta\delta_s}{2\delta}\sum_i W_i\lambda_i^2[\cos(\lambda_i\{X_c^* + \beta Y_c^*\} + \zeta_i)k_{cx,i} + \sin(\lambda_i\{X_c^* + \beta Y_c^*\} + \zeta_i)k_{sx,i}]$$

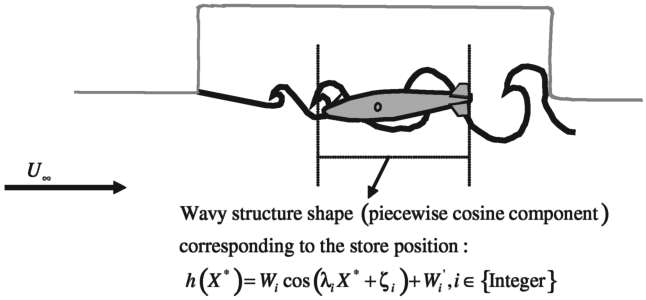

Fig. D1 Piecewise cosine wavy profile for the shear layer. The cosine component chosen here corresponds to the X' coordinate of a point on the store surface, with $X' = X_c' + \mu x$ and the nondimensionalization scheme is the same as Eq. (1).

$$g_{11} = -\frac{a(x_e)^2\delta_s}{2\delta}W_j\lambda_j\{\sin(\lambda_j\{X_c^* + \beta Y_c^*\} + \zeta_j)\cos(\lambda_j\mu x_e) + \cos(\lambda_j\{X_c^* + \beta Y_c^*\} + \zeta_j)\sin(\lambda_j\mu x_e)\}$$

$$h_{11} = -\frac{x_ea(x_e)^2\delta_s}{2\delta}W_j\lambda_j\{\sin(\lambda_j\{X_c^* + \beta Y_c^*\} + \zeta_j)\cos(\lambda_j\mu x_e) + \cos(\lambda_j\{X_c^* + \beta Y_c^*\} + \zeta_j)\sin(\lambda_j\mu x_e)\} \tag{D2}$$

The rest of the parameters are zero. It is to be noted that this contribution of the wavy profile is added to Eq. (9) to get the complete expressions for normal force and moment in the thick shear case. Also, the index j in Eq. (D2) corresponds to x_e and

$$k_{c,i} = \int_x \cos(\lambda_i\mu x)a(x)^2 \,\mathrm{d}x, \qquad k_{s,i} = \int_x \sin(\lambda_i\mu x)a(x)^2 \,\mathrm{d}x,$$
$$k_{cx,i} = \int_x \cos(\lambda_i\mu x)a(x)^2x \,\mathrm{d}x, \qquad k_{sx,i} = \int_x \sin(\lambda_i\mu x)a(x)^2x \,\mathrm{d}x,$$
$$k_{cxx,i} = \int_x \cos(\lambda_i\mu x)a(x)^2x^2 \,\mathrm{d}x, \qquad k_{sxx,i} = \int_x \sin(\lambda_i\mu x)a(x)^2x^2 \,\mathrm{d}x \tag{D3}$$

Here the integrations are carried over that portion of the store which corresponds to the piecewise cosine component represented by the index i of the wavy profile. This is illustrated in Fig. D1.

In the derivations outlined above, care was taken to include the effect of additional vertical velocity on the body surface (leading to increase in local angle of attack) as induced by the wavy shear layer profile.

Appendix E: Nondimensional Scheme Used in Different Store Drop Models

The complete set of nondimensional parameters involved in computing $\hat{F}$ and $\hat{M}$ is outlined as

$$X = \frac{\hat{X}}{\hat{l}_o}, \quad Y = \frac{\hat{Y}}{\delta\hat{l}_o}, \quad Z = \frac{\hat{Z}}{\delta\hat{l}_o}, \quad t = \frac{U_\infty\hat{t}}{\hat{l}_o}, \quad x = \frac{\hat{x}}{\hat{l}_o},$$
$$y = \frac{\hat{y}}{\delta\hat{l}_o}, \quad z = \frac{\hat{z}}{\delta\hat{l}_o}, \quad a = \frac{\hat{a}}{\delta\hat{l}_o}, \quad H_o = \frac{\hat{H}_o}{\delta\hat{l}_o}, \quad D_o = \frac{\hat{D}_o}{\delta\hat{l}_o},$$
$$\alpha = \frac{\hat{\alpha}}{\delta}, \quad H = \frac{\hat{H}}{\delta\hat{l}_o} = Y_c - \alpha x, \quad V_c = \frac{\hat{V}_c}{\delta U_\infty}, \quad \omega = \frac{\hat{\omega}\hat{l}_o}{\delta U_\infty} \tag{E1}$$

where Y_c, V_c, and ω are the vertical coordinate, vertical velocity, and angular velocity of the store c.g., respectively. The reference frame for integration is attached to the store axis and is illustrated in Fig. E1.

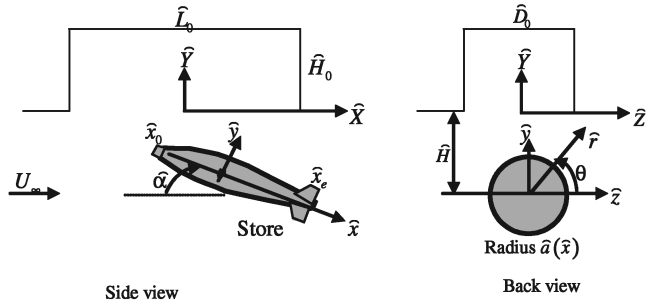

Fig. E1 Reference frames (both fixed to the store and inertial) for computing $\hat{F}$ and $\hat{M}$ on store.

Acknowledgements

This research was supported by a Defense Advanced Research Projects Agency (DARPA) grant (technical monitor, Steven Walker) through a subcontract from The Boeing Company (technical monitor, William Bower), and their cooperation is highly appreciated. The authors would like to acknowledge A. Ghoniem, J. Paduano, K. Willcox, and J. Peraire of the Massachusetts Institute of Technology (MIT) for their invaluable comments and suggestions throughout the course of the store model development. The authors also gratefully acknowledge Val Kibens, Norm Malmuth, and the reviewers for their comments and suggestions which significantly improved the paper. The discussion about the relative effects of the shear layer and store motion induced potential on the loads with the reviewers was particularly enlightening.

References

[1] Shalaev, V. I., Fedorov, A. V., and Malmuth, N. D., "Dynamics of Slender Bodies Separating from Rectangular Cavities," *AIAA Journal*, Vol. 40, No. 3, 2002, pp. 517–525.

[2] Shalaev, V., Malmuth, N., and Fedorov, A., "Analytical Modeling of Transonic Store Separation from a Cavity," AIAA Paper 0004, 2003.

[3] Bower, W. W., Kibens, V., Cary, A. W., Alvi, F., Raman, G., Annaswamy, A., and Malmuth, N., "High-Frequency Excitation Active Flow Control for High-Speed Weapon Release (HIFEX)," AIAA Paper 2004-2513, June 2004.

[4] Kibens, V., Alvi, F., Annaswamy, A., Raman, G., and Bower, W. W., "High-Frequency Excitation (HIFEX) Active Flow Control for Supersonic Weapon Release," *Proceedings of the 1st AIAA Flow Control Conference*, AIAA, Reston, VA, June 2002.

[5] Alvi, F., Annaswamy, A., Bower, W., Cain, A., Kibens, V., Krothapalli, A., Lourenco, L., and Raman, G., "Active Control of Store Trajectory in a Supersonic Cavity," *Reactive Gas Dynamics Laboratory Seminar Series*, Massachusetts Institute of Technology, March 2004.

[6] Malmuth, N., and Shalaev, V., "Theoretical Modeling Of Interaction of Mulitple Slender Bodies In Supersonic Flows," AIAA Paper 1127, 2004.

[7] Davids, S., and Cenko, A., "Grid Based Approach to Store Separation," AIAA Paper 2418, 2001.

[8] Wei, F.-S. J., and Gjestvang, J. A., "Store Separation Analysis of Penguin Missile From the SH-2G Helicopter," AIAA Paper 0992, 2001.

[9] Zhuang, N., Alvi, F. S., Alkislar, M. B., Shih, C., Sahoo, D., and Annaswamy, A. M., "Aeroacoustic Properties of Supersonic Cavity Flows and Their Control," AIAA Paper 2003-3101, 2003.

[10] Liepmann, H. W., and Roshko, A., *Elements of Gasdynamics*, Dover Publications, Inc., New York, 2001.

[11] Malmuth, N., "Theoretical Aerodynamics in Today's Real World, Opportunities and Challenges," AIAA Paper 2005-5059, Sec. IVC, p. 15.

[12] Bjorge, S. T., Reeder, M. F., Subramanian, C., and Crafton, J., "Flow Around an Object Projected from a Cavity into a Supersonic Freestream," AIAA Paper 2004-1253, 2004.

[13] Sahoo, D., Annaswamy, A. M., Zhuang, N., and Alvi, F. S., "Control of Cavity Tones in Supersonic Flow," AIAA Paper 2005-0793, 10–13 Jan. 2005.

X. Zhong
Associate Editor